Octopamine and Tyramine Modulate Motor Program Competition in *Drosophila* larvae

William V. Smith[1] and Stefan R. Pulver[1¶]

[1] School of Psychology and Neuroscience, University of St Andrews, St Mary's Quad, South Street, St Andrews KY16 9JP, UK

[¶] Corresponding author: sp96@st-andrews.ac.uk

Abstract

Dynamic Interactions amongst competing motor programs shape behavioural output. Here, we use a combination of opto- and electro-physiology to explore how the *tdc*$^{2+}$ adrenergic-like system modulates competition amongst central pattern generating (CPG) networks controlling locomotion in 3rd instar *Drosophila* larvae. Bath application of octopamine (OA) promoted fictive forwards locomotion, suppressed backwards locomotion, and induced bouts of fictive head sweeps during wash period that were proportional to the promotion of forward waves. In contrast, tyramine (TA), the conceptualised inhibitory antagonist to OA, promoted collisions and overlap of motor programmes, activity-dependent inhibition, and bouts of silence during wash periods. Dual-colour calcium imaging of the *tdc*$^{2+}$ system with motor neurons revealed that the *tdc*$^{2+}$ neurons are recruited phasically prior to a majority of fictive locomotor behaviours. Optogenetic manipulation of the *tdc*$^{2+}$ system recapitulated a subset of effects and further revealed that activity in *tdc*$^{2+}$ system neurons necessary and sufficient for locomotor CPG activity in the system. Overall, our work generates testable predictions for future behavioural and connectome-constrained computational studies for *Drosophila* motor competition and provides insights into how adrenergic-like systems can modulate dynamics of motor competition among interacting CPGs within locomotor networks.

Introduction

Effective locomotion depends on neural circuits that achieve a dynamic balance between stability and flexibility. Motor behavior arises not only through the initiation of specific motor programs but also through the suppression of pattern generation circuits that would induce alternative motor programs – motor competition [1]. Coordinated locomotion requires the sustained activation of central pattern generators (CPGs) in concert with precisely timed inhibition of premotor networks that drive opposing CPG activity. Disruption of inhibitory interactions between CPG networks can therefore lead to uncoordinated or dysrhythmic motor output [1]. To preserve both stability and adaptability, motor systems must support the initiation and maintenance of locomotor activity while retaining the capacity to transition between alternative motor programs as conditions change. Conceptually, distinct pattern-generating networks can be viewed as competing for control within a temporally constrained neural landscape to produce context-appropriate motor output. Because motor adaptability is essential for survival—for example, during rapid escape responses—understanding how motor circuits modulate and arbitrate such motor competition may reveal general principles of neural flexibility and resilience. Although the circuit motifs underlying motor program selection and coordination are increasingly well characterized (e.g., [2]), the neuromodulatory mechanisms governing competitive selection among motor programs remain comparatively unresolved.

The adrenergic-like system in *Drosophila* provides a powerful testbed to evaluate motor competition by enabling controlled, acute induction of motor bias. The *Drosophila* adrenergic-like system is composed of octopamine (OA) - an invertebrate analog to adrenaline - and tyramine (TA) [3]. The biosynthetic pathways of OA/TA, their receptor pharmacology [4], [5], and the expression patterns of OA and TA neurons are well studied in multiple invertebrate species [4], [6], [7], [8], [9], [10]. The adrenergic-like system has been implicated in a variety of fundamental behaviours including learning and memory [11], [12], social behaviours like aggression [13], [14], [15], motor initiation and modulation [9], [16], [17], [18], [19], including fundamental processes underlying action like energy metabolism [20], [21], synaptic plasticity [22], [23], and activity-mediated adaptation [24], [25]. The adrenergic-like system is consequential to invertebrate movement especially in its capacity to modulate selection of motor programs based both internal states and external sensory drives.

Traditionally, OA and TA are considered neuromodulators with opposing actions and outcomes [9], [26], [27]. Namely, OA has a well-documented promotive and facilitatory role in locomotion [9], [16], [17], [18], [27], [28], [29], [30], [31], [32] while TA appears to have an overall inhibitory effect on locomotion [6], [8], [27], [33], [34] across invertebrates. However, the functional relationship between OA and TA's action is not always exclusively antagonistic nor definitely excitatory/inhibitory. For instance, the mutual-antagonistic relationship of OA/TA appears to be conditional on their mutual relative concentrations [26]. Further, OA and TA are not always excitatory or inhibitory, respectively. For example, octopamine can have inhibitory effects on CPG activity through inhibition of CPG command interneurons [35], can inhibit nerve-based locomotion stimulation [36], and can inhibit synaptic transmission at the *Drosophila* larval neuromuscular junction [37]. Indeed, different OA receptors are linked to either stimulatory (Octβ2R) or inhibitory (Octβ1R) cAMP/CREB pathways which – a feature undermining self-regulated octopaminergic synaptogenesis at the larval neuromuscular junction [23]. On the other hand, TA can have excitatory effects on neural networks underpinning behaviour. For example, TA can evoke depolarisation through an indirect DA-mediated pathway in rat subthalamic neurons [38], at low concentrations in hyperpolarized states increase the amplitude of locust oviduct excitatory junction potentials stimulating rhythmic contractions [39], and facilitate sensitisation by delaying cocaine-induced responsive hypoactivity [40]. Nonetheless, a significant body of work points to a binary perspective on OA/TA within locomotory systems. One cause of this perspective may be that a majority of prior studies on adrenergic-like modulation have utilised powerful genetic tools (e.g., RNAi, genetic ablation) that often induces long-term changes in the neuromodulatory environments and likely induce undetermined compensation processes during development [41]. Given the highly adaptive, redundant, and complex nature of neural systems, a diverse array of system configurations and features can be somewhat divorced from their ecological

contexts [42], [43], [44]. Consequently, chronic genetic manipulations may induce outcomes with complicated interpretations. In contrast, acute modulation of adrenergic-like signalling gives insights into effects that occur moment-to-moment and are not confounded by compensation due to changes in gene expression.

The adrenergic-like system has been well characterised and documented in *Drosophila* larva. Within *Drosophila*, tyrosine is converted to tyramine through tyrosine decarboxylase (TDC) and tyramine is then synthesised into octopamine through tyrosine-β-decarboxylase (TβH). Of the two isoforms of TDC, exclusively tdc^{2+} expresses in neurons [45], [46], [47]. Through immunohistochemistry of $tdc^{2+}$and TβH [9], [48], we have a good understanding of OA- and TA-manufacturing neurons within the *Drosophila* larva (see Figure 1 for larval anatomy summary from Selcho's work). Noteworthily, not all TDC-expressing neurons stain for both tyramine and octopamine; a large subset of tdc^{2+}-expressing neurons appear to exclusively release octopamine [9]. In the *Drosophila* larval ventral nerve cord, one pair of ventral-paired medial neurons (Figure 1, green) are exclusively tyramine releasing. Conceptually, the set of tdc^{2+}-expressing neurons can be segregated into descending and ascending connections with the majority of abdominal tdc^{2+} octopamine neurons (OANs) sending exclusively local-terminating ascending projections. Given the high level of characterisation of the adrenergic-like system in *Drosophila* [48] and the transferability of larval fictive activity to understanding intact locomotion [49], [50], we elected to manipulate the activity of tdc^{2+}-expressing neurons to evaluate the effects of intrinsic OA/TA on motor competition within *Drosophila* 3rd instar larvae.

The role of the adrenergic-like system in modulating action selection and motor pattern competition has been extensively studied in *C. elegans* through tyraminergic RIM neurons [51], [52], [53] which has instantiated a fundamental adrenergic-like motif (i.e., "master-and-slave") in *C. elegans* locomotion. However, while the role of OA/TA has been studied in *Drosophila* with reference to specific motor program initiation and coordination [54], limited work has been conducted on their coordinated role to generalisable motor competition. Through studying the effects of acute modulation on action selection and motor competition, we may be able to gain a more robust, nuanced, and applicable understanding of OA/TA neuromodulatory antagonism.

Here, we explore the role of the tdc^{2+} system modulating fictive motor competition in *Drosophila* larvae to better understand the neural architecture behind CPG coordination and competition. Firstly, we evaluate the modulatory activity of tdc^{2+} system neurons on isolated central pattern generators in 3rd instar *Drosophila* larvae. Specifically, we show that activity in tdc^{2+} neurons and motor neurons are highly correlated during fictive locomotion. Secondly, we demonstrate how bath-applied exogenous OA and TA induce acute changes in CPG activity during and after bath application. Specifically, OA

induces elevated fictive forward locomotion in isolated central pattern generators. In contrast, exogenous TA induces increased overlapping fictive patterns with activity-dependent inhibitory effects on general fictive activity. Both neuromodulators also induce long lasting effects following bath application that reflect activity changes in the network. Thirdly, through optogenetic manipulation of *tdc*$^{2+}$ neuronal activity, we demonstrate how *tdc*$^{2+}$ neuronal activity appears sufficient and necessary for producing fictive rhythms. Finally, we show how regionally restricted depolarisation of *tdc*$^{2+}$ neurons in the posterior abdominal isolated ganglion are sufficient to induce fictive forward activity. Overall, we demonstrate how motor competition could be a unique and important way to conceptualise motor diversity and neuromodulation and how the adrenergic-like system is a valuable tool for understanding the secondary effects of modulating motor competition.

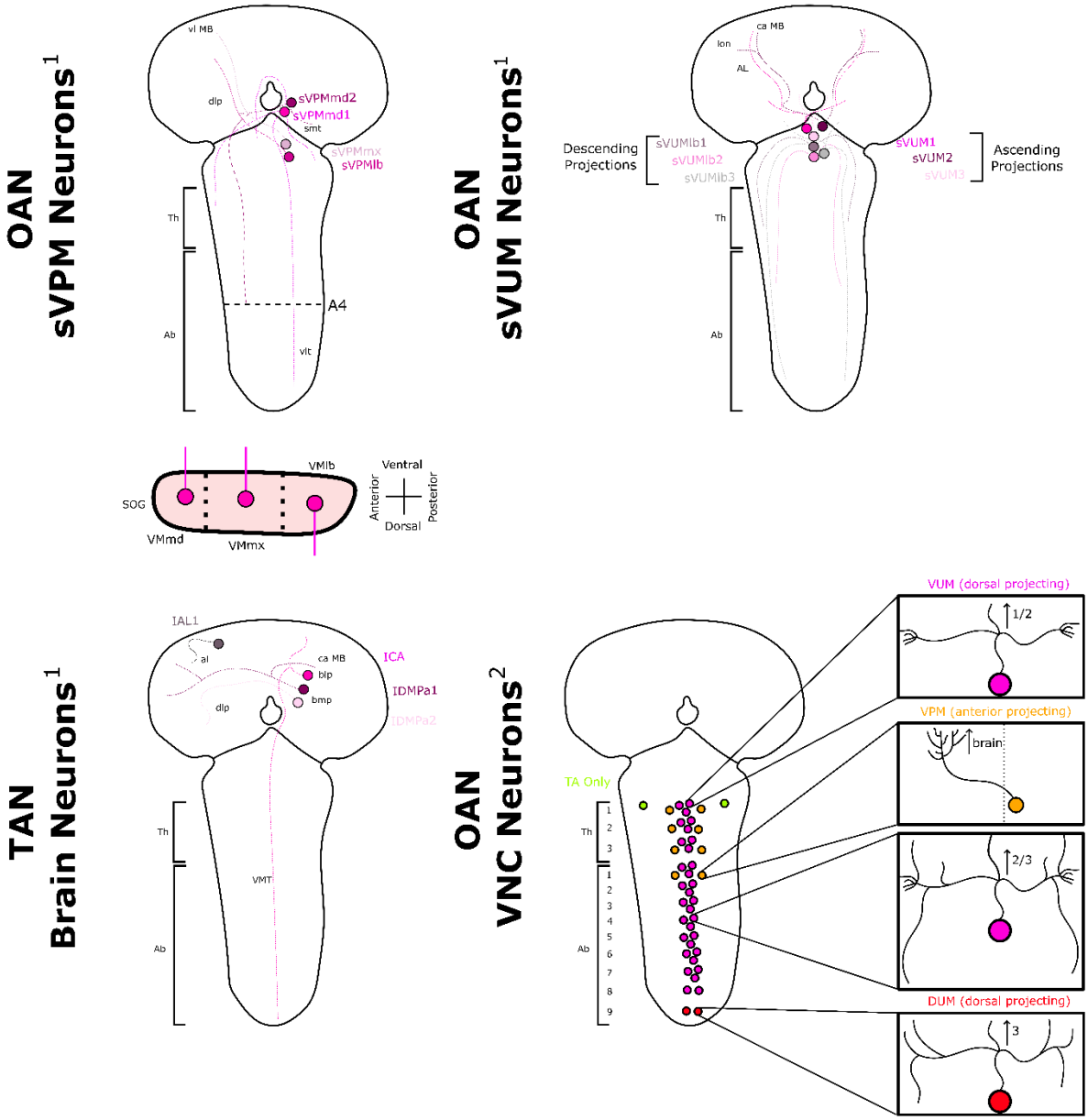

[1]*Adapted from Selcho et al., (2014)*
[2]*Adapted from Selcho et al., (2012)*

Figure 1: Summary of Octopaminergic and Tyraminergic Neurons in the *Drosophila* Larva

General cell body position, defined name, and projection patterns for the octopaminergic (OAN) and tyraminergic (TAN) neurons as characterised in [9], [48]. The OAN ventral paired median (sVPM) neurons in the suboesophageal zone (only right-side shown) have contralateral brain projection and both ipsilateral and contralateral descending ventral nerve cord (VNC) projections. The projections of OAN sVPM neurons aligns to their anterior-to-posterior cell body position as shown beneath the sVPM map. The suboesophageal zone also harbours the suboesophageal ventral unpaired median (sVUM) octopaminergic interneurons which, unlike the VNC octopaminergic neurons, primarily unction to dynamically modify sensory processing and context-dependent behaviours like arousal or odour discrimination [55]. The sVUM cluster can be classified into those octopaminergic neurons with ascending or descending projections. The vast majority of exclusively tyraminergic neurons are currently classified within the brain showing contralateral projections with predominately interbrain connections but

some tyraminergic neurons do have VNC-wide descending projections. A set of ~40 octopaminergic and 2 tyraminergic neurons almost exclusively within the VNC. As shown in the bottom right panel, OAN VNC neurons consist of ventral unpaired medial dorsal projecting, ventral paired medial anterior projecting to the brain, and dorsal unpaired medial dorsal projecting neurons. All these neurons have local ascending projections 1-3 segments anteriorly of their soma's segment. Importantly, only two neurons in [9], [48] were reported to exclusively manufacture tyramine and not octopamine with those neurons (shown in green) residing in the upper thoracic segment exclusively.

Methods

Animal Rearing & Dissection

Drosophila were raised at 18-25□C in incubators on an approximate 12-hour light-dark cycle. All experiments were conducted with feeding 3rd instar *Drosophila* larva (2-3 days post hatching). The central nervous system (CNS) of *Drosophila* was isolated as reported in [49]. Activity of isolated CNSs was recorded with Baines External Saline (BES) submersion containing (in mM) 135 NaCl, 5 KCl, 2 $CaCl_2$, 4 $MgCl_2$, 5 TES, and 36 sucrose, pH 7.15 [56]. All CNS preparations were isolated from *Drosophila* larva using dorsal incision across the larva body using fine scissors with body walls pinned into a Sylgard-lined Petri dishes using fine tungsten wires (California Fine Wire, Grover Beach, CA). All projecting CNS nerves were cut, CNS removed, posterior nerves and peripheral gastric tissue attached were pinned using fine tungsten wires (see [49]).

Dual Colour Ca^{2+} Imaging of *Tdc*$^{2+}$ and Motor Neurons

The calcium activity patterns of motor neurons and *tdc*$^{2+}$ neurons [45] were assessed in isolated CNS feeding 3rd instar *Drosophila* larva using a genetic construct that drove RCaMP1a expression in glutamatergic neurons (VGlut-LexA combined with 13XLexAOP-RCaMP1a balanced over CyO, Tb-RFP), while also containing UAS-GCaMP6f (provided by K.L. Hibbard, Janelia Research Campus) This construct was then crossed to w[*]; P{w[+mC]=Tdc2-GAL4.) Isolated CNS *Drosophila* were imaged using an OptoSplit Imaging system (Cairn Research Ltd, Kent, UK) with appropriate excitation and emission filters for RCAMP and GCAMP imaging. Preparations were imaged using an OLA light engine (Lumencor, OR, USA) and an ORCA-Fusion CMOS camera (Hamamatsu, Hamamatsu, Japan) with a XLUMPLFLN 20X dipping objective (Olympus, Tokyo, Japan). We imaged isolated dual-colour CNS *Drosophila* with BES using an X-light spinning disk confocal with a 70µm pinhole array (Crest Optics, Rome, Italy) for up to 30 minutes at 5fps with 150ms exposure. Images were collected using MicroManager (v2.0 gamma [57]) and post-processed using ImageJ [58], [59]. The channels displaying the calcium activity for motor neurons and *tdc*$^{2+}$ neurons were overlayed using each segment's nerve roots as a reference marker. All calcium signals were extracted using area-consistent regions of

interest on nerve roots projecting from ventral nerve cord segments (T3-A6) (Figure 1Aii). All calcium signals were pre-processed (df/f) and smoothed using a custom Python script (see data repositor for details) Fictive events were determined through using Hill's Valley Analysis in DataView [1] and/or SciPy's peak detection algorithm based on criteria reported in [49].

Visualisation of dual-colour calcium data was performed in DataView and Python3 using scripts available in paper-associated repositories. The overlaid average calcium activity trace in *tdc*$^{2+}$ and motor neurons (as shown in Figure 1C) was performed using DataView's event-scope view based on segregated fictive events detected by Hill's Valley analysis across all preparations based on criteria reported in [49]. The average waveform of each event was calculated by DataView and extracted into Python for across preparation visualisation. All average waveforms were determined using a duration threshold of 8300ms. The peak time lag calculation (as shown in Figure 1D) was the difference in peaks from the average waveform of *tdc*$^{2+}$ and motor neurons in each segment using SciPy's peak detection algorithm (see repository code). Fictive events in calcium traces were determined using Hill's Valley analysis and manually counted as reported in [49]. Peak and duration relation between *tdc*$^{2+}$ and motor neuron calcium signals (as shown in Figure 1G) was performed using Hill's Valley detection on each segment across all preparations with duration calculated as 20% on-off from the centre of the calcium signal. The correlation between *tdc*$^{2+}$ and motor neuron calcium signals (as shown in Figure 1E) was conducted using Pearson Cross Correlation coefficient across all preparations through Python's Scipy.Signal package (see repository code).

Ca^{2+} Imaging with Tyramine & Octopamine Perfusion

The effect of exogenous octopamine bath application on calcium signals in motor neurons was assessed in isolated CNS feeding 3rd instar *Drosophila* larvae using a genetic line in which GCaMP6m is driven in glutamatergic neurons by the OK371-GAL4 line. Isolated CNS preparations were pinned to Sylgard-lined Petri dishes as described in "Dual Colour Ca^{2+} Imaging of *tdc*$^{2+}$ and Motor Neurons". Saline and OA or TA were applied during imaging using a gravity-based perfusion system with a consistent drip inflow across preparations and removed continuously using a KCP3-B10W peristaltic pump (Kamoer 60-120 RPM). Across all preparations, saline was bath applied onto the preparation for at least 10 minutes followed by 10-minute OA or TA application then < 20 minutes saline reapplication to wash away octopamine/tyramine from the Sylgard-lined Petri dish. All OA concentration ranges (5 - 400µM) were generated from a diluted 0.02M master mix (O0250-1G Sigma Aldrich). All TA concentration ranges (5 - 400µM) were generated from a diluted 0.01M master mix (T90344-5G Sigma Aldrich). Images were collected using WinFluor (University of Strathclyde, UK) at 10fps and post-

processing using ImageJ [58], [59]. All isolated preparations were recorded using a UPlanFLN Olympus 10x, 0.3nA.

Tdc^{2+} Optogenetics

The effect of endogenous *tdc*$^{2+}$ activity on fictive motor activity was studied using extracellular electrophysiology on segmental nerve roots in isolated CNS from feeding 3rd instar *Drosophila* larvae. Octopaminergic *tdc*$^{2+}$ neurons were either depolarised using lines containing 20xUAS-CsChrimson-mVenus inserted at the attP18 landing site or hyperpolarized using lines containing UAS-GtACR1 inserted in VK00005 driven by w[*]; P{w[+mC]=Tdc2-GAL4. Across all conditions, the activity of thoracic nerve root (T3) and posterior abdominal nerve root (A6-A8) was measured by suction electrode recording (AM System Differential AC Amplifier Model (#59721, 1700), 1-100kHz cut-off frequency allowance). Borosilicate glass capillaries were pulled using an electrode puller (Narishege, Japan), and tapered tips were broken to produce suction electrodes that fit tightly around single nerve roots. Stimulation during the *tdc*$^{2+}$-CsChrimson conditions was performed with a downward-projecting red LED light source (Cairn Research Ltd., 620 nm, 0.58mW/cm^2). The stimulation period was either consistent for 10, 20, or 40s or discontinuous with 0.01s pulses generated at intervals of 40Hz for ~10s total pulsed stimulation. Stimulation during the *tdc*$^{2+}$-GtACR1 conditions was performed with upward-projecting white light (~2.5mW/cm^2). The stimulation period was consistent for ~15, 30, or 60s induced by manual instantiation. All whole-prep stimulation used full-prep illumination using a UPlanFLN Olympus 10x, 0.3nA lens.

Restricted illumination stimulation conditions involved restricting the downward-projecting red light source using a light-path restrictor with ∾0.6cm aperture and 0.16mW/cm^2 power-to-area ratio. Restricted stimulation involved a LUMPlanF Olympus 40x, (0.8 nA) dipping lens, to prevent light scattering and thus unintended illumination, focused on posterior abdominal, anterior abdominal, thoracic, and suboesophageal ganglion regions (see Figure 6). Aside from direct restricted prep stimulation, all conditions were matched with control stimulation where illumination of the left-flank of the preparation (< 1cm) was conducted during nerve root recording.

All electrophysiology recordings and light stimulations were made using LabChart 8.0 software (AD Instruments, Colorado Springs, CO) and post-processed in Spike2 (Cambridge Electronic Design, Cambridge, UK) and Python3. Post-processing involved rectification and smoothing using a consistent 0.2s time interval. All rectified and smoothed traces were imported into DataView where event peaks and 20% on-off duration were determined by Hill's Valley analysis. Visualisation and further analysis were conducted in Python3 (see repository code).

Determination of Fictive Activity

The motor dynamics within the isolated VNC preparation were classified using Hill's Valley thresholding to determine peaks within motor activity in each abdominal and thoracic ganglion segment alongside established definitions for each fictive behaviour [1], [49], [50] (see Figure 2 for visual representations of each fictive behaviour). Succinctly, fictive forward waves and fictive backward waves were determined by the existence of sequential Hill's Valley-determined peaks proceeding from either posterior-to-anterior or anterior-to-posterior in all segments, respectively. Fictive headsweeps were determined by computing a difference trace (left – right) in the T3 segment and determining anterior asymmetric activities as peaks or thoughts that exceeded ±10% absolute threshold difference. Turning behaviours were defined as anterior asymmetric activity that was the exclusive T3 event occurring before a fictive backward event. Finally, anterior symmetric (i.e., anterior burst) or posterior symmetric (i.e., posterior burst) were determined by peak detection of the left and right trace in T3-A2 and A6-8 respectively. Some anterior burst and posterior burst fictive activities are in varying numbers of anterior and posterior segments thus any peak detection in both the left and right trace within 5s of each other was determined as symmetric activities of each definition. In the calcium dataset, Hill's Valley peak detection was performed after baseline smoothing within DataView [1]. In the electrophysiology dataset, raw electrophysiological traces were smoothed in Spike2 thereafter DataView was used to determine peaks in the anterior and posterior trace akin to the calcium dataset analysis pipeline. Specifically, the determination of fictive forward vs backward activity was determined by the minimum peak-to-peak time between the initiating-vs-terminating segment. Specifically, if the peak time difference between T3-to-A8 was shorter than the peak time between A8-to-the-next-T3 peak then the activity peaks were classified as fictive backward events rather than fictive forward events. If the activity peak differences exceeded 3s, the activity peaks were either reported as anterior bursting or posterior bursting events in T3 or A8, respectively. In cases of ambiguity, the fictive events were not recorded. Manual corrections – deletions or additions of peaks – were performed, when necessary, in line with the strict fictive definitions highlighted above.

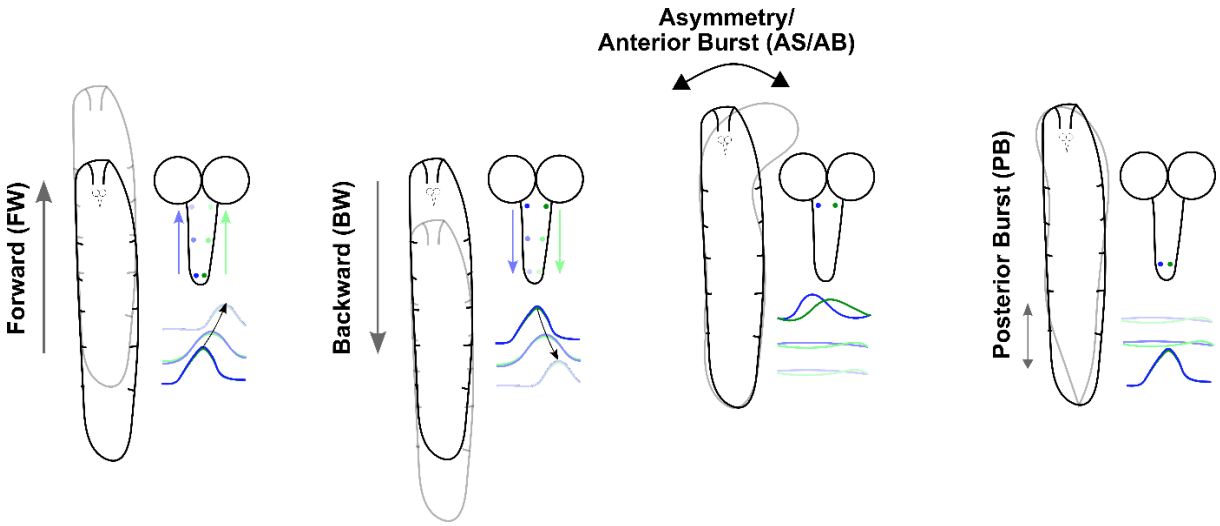

Figure 2: Summary of Larval and Fictive Behavioural Categories

The intact behaviour of the *Drosophila* larva is represented by different motor neuron activity sequences within the isolated ventral nerve cord (as originally noted in [49], [50]). All subsequent calcium imaging analysis categorises sequential motor activity in either of the five fictive patterns: fictive forward (FW), fictive backward (BW), anterior asymmetric (AS), anterior bursting (AB), or posterior bursting (PB) events. Each motor pattern is shown with its intact and isolated ventral nerve cord companion.

Activity, silence, and overlap incidence for the tyramine perfusion analysis was conducted in DataView with strict definitions. The duration of total fictive activity was determined through the same Hill's Valley peak detection algorithm used to initially categorise fictive activity patterns. Specifically, the total duration of fictive activity within a condition time was calculated as the 80% margins before and after peaks in calcium activity from all segments that exceeded 10% standard deviation above the baseline signal. Silence was determined by the total time of each condition's recording period subtracted by the duration of total fictive activity. Fictive overlap was defined as the existence of the start, or progression, of a fictive behavioural program in the network before the definitional completion of a prior fictive program. For instance, a fictive forward wave would be overlapping a fictive backward wave if the A8 initiation peak of the fictive forward wave occurring before the T3 completion peak of the fictive backward wave. Exclusively fictive wave motor programs were considered in the definition of overlapping fictive events.

Analysis, Visualisation, & Statistical Evaluation

All calcium signal and electrophysiology nerve root data were initially analysed in DataView (version 12.2.2)[60] using Hill's Valley Analysis for peak detection and Event-Triggered Scope View for averaging waveforms. All data were visualised in Python3 using custom scripts available in the repository supplied by the authors. All statistical tests were performed using packages within Python (see repository scripts and report tests in the results sections).

Results

Tdc^{2+} VNC Neuron Activity is Correlated to Motor Neuron Activity across all Fictive Motor Programs

The isolated *Drosophila* central nervous system (CNS) spontaneously generates motor rhythms (denoted as "fictive" to distinguish from intact motor programs) in the thoracic and abdominal segments that can be measured via calcium indicators expressed in neuronal populations [49]. Previous work has characterised the features and relationship between fictive activity patterns using different genetically-encoded calcium indicators [1], [49], [50], [61]. Succinctly, isolated CNS preparations display fictive forwards and backwards motor programmes characterised by anterior-to-posterior or posterior-to-anterior progression of activity in motor neuron segments, respectively. In addition, preparations also can display fictive bilaterally symmetric activity in the anterior thoracic and posterior abdominal segments indicative of head raising or tail grounding behaviours, respectively. Finally, preparations can display bilaterally asymmetric activity in the anterior thoracic indicative of headsweep-like behaviours in intact *Drosophila* larva (Figure 3Ai). Octopamine (OA) is manufactured and released from neuronal subpopulations in the suboesophageal ganglion and ventral nerve cord expressing the *tdc*$^{2+}$ gene [9] with staining suggesting the brain contains only TA, and no OA-immunoreactive cells [46]. Given both chronic and acute manipulations can have a profound effect on locomotion, we first evaluated if activity of OA neurons in the ventral nerve cord (VNC) – indicative of predominately OA release – was correlated with fictive motor rhythms. There exist subpopulations of distinct octopaminergic neurons that line the ventromedial (T3-A6) axis of the CNS [9]. Through expressing different calcium indicators in VNC motor neurons (VGlut, RCaMP1a) and ventromedial *tdc*$^{2+}$ neurons (TDC^{2+}, GCaMP6f) (Figure 3Aii), we explored the intrinsic activity relationship between VNC *tdc*$^{2+}$ neurons and motor neurons during spontaneous fictive activity bouts. The calcium activity of motor neurons and *tdc*$^{2+}$ neurons in each VNC segment showed high correlation across different fictive motor programs (Figure 3B).

By parsing all instances of fictive events across dual-colour preparations (N=7), we can see a robust similarity in *tdc*$^{2+}$ and motor neuron temporal activity within each segment (Figure 1C). Specifically, if we take the average calcium activity trace for all segments for motor neurons and *tdc*$^{2+}$ neurons across fictive activity patterns, we see motor neuron *tdc*$^{2+}$ neurons activity has a consistent similarity and phase locking. The strong activity association between motor neurons and *tdc*$^{2+}$ neurons is further apparent when comparing activity peaks between each neuronal population in each segment per each unique fictive behaviour (Figure 3D). The temporal relationship between motor neuronal and *tdc*$^{2+}$ neurons showed variations depending on the fictive motor program. At the initiating segment for

fictive activity, motor neuron activity on average preceded *tdc*$^{2+}$ neuron activity for fictive forward (462±704 ms at A6, N=5), posterior burst (449±614 ms at A6, N=5), and anterior burst (235±352 ms at T3, N=2) fictive events. In contrast, *tdc*$^{2+}$ neuron activity preceded motor neuron activity in initiating segments for fictive backward (432±786 ms at T3, N=3), right asymmetric (9±38 ms at T3, N=2), and left asymmetric (99±57ms at T3, N=3) events. Importantly, the time phase relationship between motor neurons and *tdc*$^{2+}$ neuron activity at initiation is not always held consistently in all ganglion segments as the activity pattern progresses through the VNC. For example, as fictive forward motor activity progresses to the anterior regions (A2 - T3) of the CNS, average *tdc*$^{2+}$ neuron peak activity now precedes motor neuron activity (Figure 2C, D). In short, while there is some inter-prep variability between the temporal organisation of motor neuron and *tdc*$^{2+}$ neuron peak activity, there is a strong coupling between the activity of these two neuron subpopulations in all fictive behaviours; in all fictive patterns, there is a system-wide mirror-image of activity across all segments even if the lag relationships show intersegmental differences.

Tdc^{2+} neurons show activity patterns both commensurate with but also independent of motor neuron activity. The majority of fictive motor events across preparations showed commensurate *tdc*$^{2+}$ neuron activity events. Across all preparations, 69% of fictive forward waves and anterior asymmetric events, 76% of posterior burst events, and 100% fictive backward waves showed commensurate *tdc*$^{2+}$ activity in a close time window (< 5s) and same segment-to-segment relationship that classically defines the fictive motor programs (Figure 1E). Notably, there was a large variability in recruitment between preparations that underestimates the overall level of recruitment displayed by some preparations. Nonetheless, in 4 out of 6 preparations, there was >90% fictive forward recruitment. In short, most fictive motor patterns have commensurate *tdc*$^{2+}$ neuron patterns but there are excess motor patterns not matched in *tdc*$^{2+}$ patterns. Similarly, there are excess fictive-like *tdc*$^{2+}$ activity patterns that occur without commensurate fictive motor patterns in the network (Figure 3F). Across preparations, there are excess *tdc*$^{2+}$ activity patterns reminiscent of all types of fictive-like activity events. Across all preparations there were 7.8% more backwards-like activity patterns in *tdc*$^{2+}$ neurons than backward fictive motor activity patterns despite 100% recruitment per preparation. Similarly, per preparation, there were 8.7%, 5.4%, 1.8%, 2.1% excess *tdc*$^{2+}$ recruitment for anterior burst, anterior asymmetric, fictive forward, and posterior burst activity, respectively.

Independent of fictive events, the activity in motor neurons and *tdc*$^{2+}$ neuron pools per segment are highly correlated. Specifically, the quantity of motor neuron and *tdc*$^{2+}$ neuron calcium activity peaks (r_s = 0.82, $p < .001$) (Figure 3Gi) and duration (r_s = 0.81, $p < .001$) (Figure 3Gii) of activity within each segment were highly correlated. Pearson correlation between motor neuron and *tdc*$^{2+}$ neuron calcium

activity per segment demonstrated an average, moderately positive correlation (r = 0.4) but with considerable intersegmental and lateral variability (Fisher's Z Score = 0.44 with 0.27 variance). Overall, activity of motor neurons and *tdc*$^{2+}$ neurons are highly correlated. When fictive motor events occur, there is likely a commensurate, almost synchronous *tdc*$^{2+}$ signal as the event propagates in the VNC.

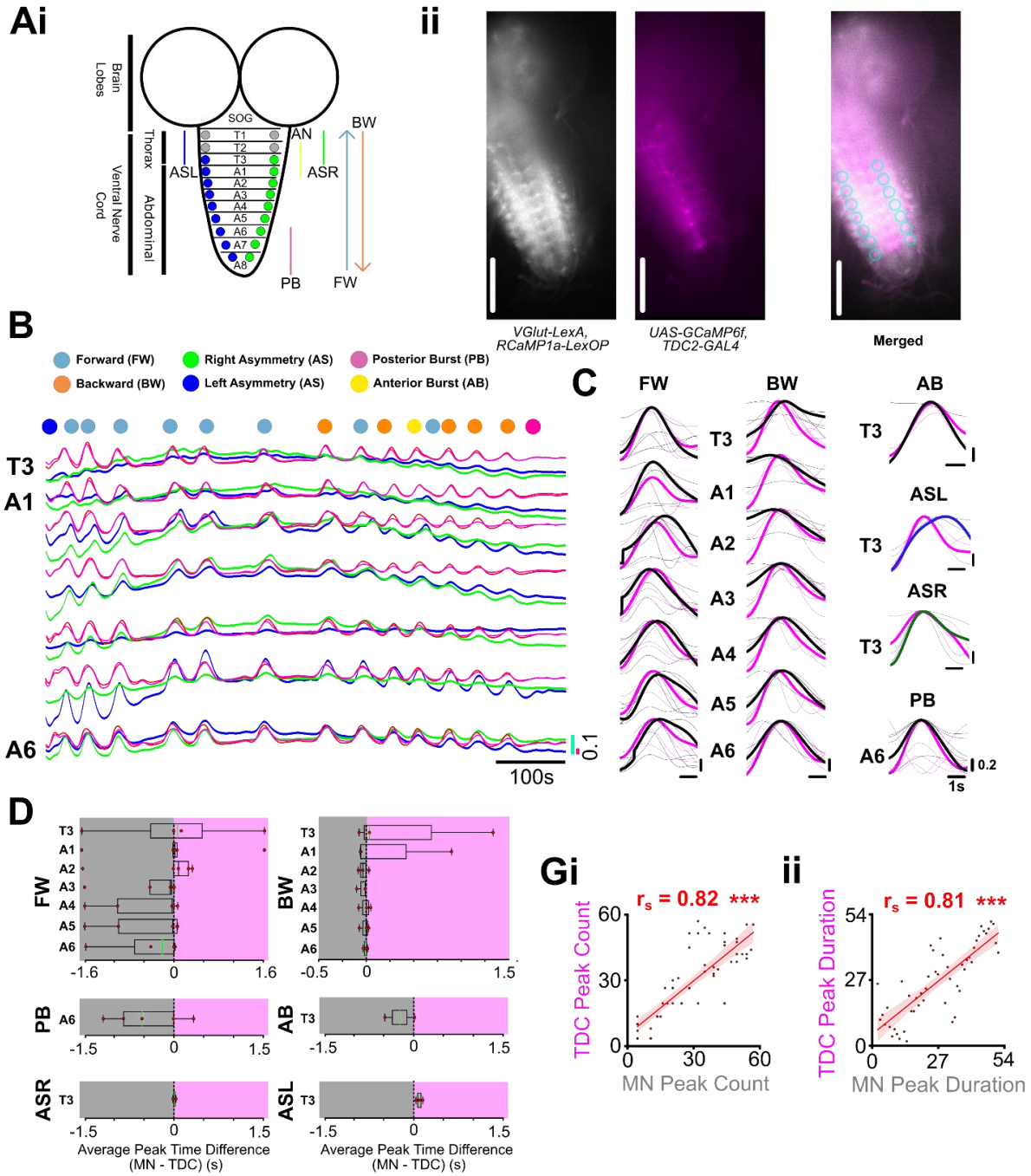
Ai
Brain Lobes
Ventral Nerve Cord
Thorax
Abdominal
SOG
T1
T2
T3
A1
A2
A3
A4
A5
A6
A7
A8
AN
ASL
ASR
BW
PB
FW
ii
VGlut-LexA, RCaMP1a-LexOP
UAS-GCaMP6f, TDC2-GAL4
Merged
B
Forward (FW)
Backward (BW)
Right Asymmetry (AS)
Left Asymmetry (AS)
Posterior Burst (PB)
Anterior Burst (AB)
T3
A1
A6
100s
0.1
C
FW
BW
AB
ASL
ASR
PB
1s
0.2
D
Average Peak Time Difference (MN - TDC) (s)
Gi
ii
r_s = 0.82 ***
r_s = 0.81 ***
TDC Peak Count
MN Peak Count
TDC Peak Duration
MN Peak Duration
E
Recruitment (%)
Fictive Behaviour
F
MN
TDC
Behaviour
Event Count
H
L
R
Segment
Correlation

364

Figure 3 High Activity Correlation between *tdc*$^{2+}$ VNC and Motor Neurons in the Same Segment and Fictive Pattern

(**Ai**) The isolated ventral nerve cord (VNC) demonstrates sequences of motor neuron activity resembling activity patterns underlying locomotion in intact animals (i.e., "FW" = fictive forward, "BW" = fictive backward, "AB" = anterior burst, "PB" = posterior burst, "ASR" = asymmetric right, "ASL" = asymmetry left). (**Aii**) Intrinsic calcium activity of motor neurons (MN) and octopaminergic neurons (*tdc*$^{2+}$) is evaluated through dual calcium indicator expression at nerve root regions of interest (blue circles) T3 - A6. Dots above the traces indicate the initiation of the different fictive behaviours (light blue, fictive forward; orange, fictive backward; yellow, anterior symmetric burst; pink, posterior burst; blue, left anterior asymmetry; green, right anterior asymmetry). Lines indicate baseline-correct calcium fluorescence values (green/blue = right/left MN in each segment, magenta/red = right/left *tdc*$^{2+}$ VUM in each segment) (**B**) Exemplar calcium trace of MN (left = blue, green = right) and *tdc*$^{2+}$ neurons (left = magenta, right = red) demonstrating strong association between MNs and Tdc2+ neuron activity within each ventral nerve cord (VNC) segment. (**C**) Averaged calcium image traces of *VGlut RCaMP1a* (black), *Tdc2*$^{+}$ *GCaMP6f* (magenta) for fictive forward (FW), backward (BW), anterior burst (AB), left asymmetry (blue, ASL), right asymmetry (green, ASR), and posterior burst (PB) activity. Bold traces represent average across all preparations (N = 7) with each individual prep average calcium trace in non-bold. The calcium signal amplitudes are normalised within each fictive behavioural class. (**D**) The time difference between the peaks in the MN and TDC calcium trace within each preparation, across fictive patterns and ventral nerve cord segment (T3 - A6). Negative average peak time differences occur when the average prep MN trace proceeds the TDC signal in the segment, positive average peak time represents TDC proceeding MN signals in the segment. Green line represents the average peak time difference across all preparations in the most distal VNC segments. (**E**) The % event count where a motor neuron fictive pattern exists alongside a corresponding TDC activity pattern across different fictive activity categories (with standard error bars). (**F**) The count of fictive activity patterns demonstrated by MN and TDC VNC populations. Note in many fictive activity patterns there is an excess of TDC exhibitions compared to motor fictive patterns. (**G**) An agnostic measure of MN and TDC signals pooled across segments and preparations showing the Spearman's Rank for (**i**) peak count comparison and (**ii**) 20% on-off peak duration comparison. (**H**) Pearson correlation coefficient for the MN and TDC traces of each segment within all preparations for the left (blue) and right (green) axis of the VNC. Comparisons followed by post-hoc was conducted with p-values: < .5 (*), < .01 (**), <.001 (***) shown. Only statistically significant bars are shown.

Bath Application of OA induces Fictive Forward & Long-lasting Anterior Asymmetric Activity

Given the high correlation between *tdc*$^{2+}$ neuron and spontaneous motor activity, we next turned to evaluate the effects of OA on fictive motor bouts. Exogenous application of OA to intact invertebrates has a well-reported role as a promoter of locomotion aligned with fight-or-flight responses [4], [11]. Here, we explored how exogenous application of OA shapes isolated locomotory networks devoid of sensory feedback to better understand the role of OA on coupled oscillatory circuits and motor competition.

The exogenous application of OA altered the fictive landscape demonstrated by the isolated VNC preparation, moving the isolated system from producing a diverse range of fictive behaviours to nearly exclusively fictive forward motor patterns (Figure 4A). Application of OA concentrations ≥100µM

405 significantly promoted fictive forward activity (100µM 5.4±2.0m^{-1} p = .003; 200µM 6.5±3.2m^{-1} p <
406 .001; 400µM 14.9±6.4m^{-1} p = .004) compared to saline pre-application (100µM 0.7±0.4m^{-1}; 200µM
407 0.7±0.7m^{-1}; 400µM 0.8±0.7m^{-1}) (Figure 4Bi). At OA concentrations ≥200µM, the induction of fictive
408 forward bias came at the expense of fictive backward motor activity which was significantly reduced
409 (200µM 0.2±0.6m^{-1} p = .005; 400µM 0.6±0.7m^{-1} p = .004) compared to saline pre-application (200µM
410 1.4±0.5m^{-1}; 400µM 2.3±0.9m^{-1}) (Figure 4Bii). Interestingly, anterior asymmetric events were
411 significantly promoted at higher OA concentrations >400µM (Figure 4Bv). However, the significant
412 elevation in anterior asymmetric activity was not induced during the 10-minute OA application but
413 only after the OA was washed from the preparation and thus consequent to the neuromodulator-
414 induced fictive forward bias (Figure 4A, Bv). Importantly, while OA did not appear to significantly
415 potentiate anterior asymmetric fictive activity in a concentration-dependent manner, there was a
416 trend to increased anterior asymmetric activity with increasing OA concentration. Interestingly, OA
417 induced long-lasting elevated anterior asymmetric activity with a frequency peak 35.7±16.9 minutes
418 post the start of the OA wash period. Noteworthily, as anterior asymmetric activity is not promoted
419 at lower OA concentrations, we can be confident that the post-application effects are not an artefact
420 of diminishing OA during the gradual wash period. By exploring fictive transitions (i.e., the probability
421 of making a transition from one motor program to another), we can see that OA-induced forward bias
422 is reflective of a significant decrease in fictive transitions programs that would transition the network
423 away from fictive forward motor patterns thereby persisting the incidence of fictive forward activity
424 (Supplementary Figure 1B). Overall, exogenous application of OA appears to collapse fictive activity
425 diversity, tuning the network into fictive forward bias mode with consequent post-application motor
426 bias to non-wave-like activity.

427 To understand the relationship between OA's induction of fictive forward bias and the post-
428 application anterior asymmetric fictive activity, we examined the relative changes in fictive frequency
429 between different motor programs across all concentrations (Figure 4D). Intriguingly, the more
430 exogenous OA promoted fictive forward bias, the greater the post-application anterior asymmetric
431 activity relative to pre-application (Figure 4Di, r_s = 0.5, p < .001). This proportional relationship was
432 not exhibited between any other fictive event. Interestingly, the proportional increase in anterior
433 asymmetric activity with respect to fictive forward bias appears significantly conditional on the relative
434 promotion of anterior asymmetric activity during OA application (Figure 4Dii, r_s = -0.4, p = .002). Put
435 simply, the greater fictive forward bias promoted by OA, the more fictive anterior asymmetric activity
436 is delayed until the network is no longer forward biased (Figure 4Dvi ,R^2 = 0.4 p < .001). In effect, it
437 appears that post-OA promotion of anterior asymmetric events is a product of OA evoking greater
438 fictive forward bias in the isolated preparation at the expense of anterior asymmetric events. During

439 OA application, the induced fictive forward bias is regularly interspersed with a few anterior
440 asymmetric events implying while OA potentiates the network towards fictive forward activity it does
441 not completely suppress anterior asymmetric activity (Figure 4A, Octopamine, "FW // AS Transitions").
442 Taken all together, this implies that fictive forward bias immediately potentiates anterior asymmetric
443 activity, but the former dominates in isolated VNC output over the latter until OA's removal removes
444 the neuromodulatory potentiation of fictive forward activity.

445 Aside from changes in the frequency of fictive events at the CPG level, OA induces significant decrease
446 in the amplitude of the calcium signal without a noticeable change in signal baseline as previously
447 reported by [62] (Figure 4Aii, Supplementary Figure 1A-E). The reduction in calcium amplitude was
448 reflected by a reduced duration in motor root bursting during OA application in both thoracic and
449 abdominal motor pools demonstrating the amplitude change in the calcium signal is reflective of OA-
450 induced shorter motor neuron bursting (Supplementary Figure 1F-H).

451 We next evaluated how the OA-induced faster rhythms exhibited in intact *Drosophila* [27] are
452 represented in the isolated motor circuit. Exogenous bath application of OA qualitatively decreased
453 intersegmental propagation delay for fictive forward and turn but not fictive backward activity (Figure
454 4C). Fictive forward wave (Figure 4Ci) and turn wave (Figure 4Ciii) duration is significantly shorter with
455 exogenous OA application. Specifically, all OA concentrations ≥50µM significantly increased forward
456 wave speed (50µM 4.4±2.4s $p = .05$; 100µM 3.6±1.3s $p < .001$; 200µM 3.7±1.4s $p = .002$; 400µM
457 1.7±0.7s $p = .01$) compared to pre-application saline perfusion (8.4±8.3s). Similarly, octopamine
458 concentrations ≥200µM significantly increased turn wave speed (200µM 3.2±1.6s $p = .01$; 400µM
459 1.6±1.4s $p = .03$) compared to pre-application saline perfusion (7.0±1.9s). OA did not induce any
460 significant changes in fictive backward wave speed. Thus, OA biases the isolated *Drosophila* CNS to
461 fictive forward locomotion consequently restricting motor diversity, induces faster CPG bursting, and
462 potentiates intersegmental propagation between segments that affects some system-wide activity
463 progression. More subtly, given that lower OA concentrations could significantly affect selective
464 intersegmental propagation but not overall fictive frequency, these data imply OA can modulate
465 locomotory speed independent of modulating initiation bias.

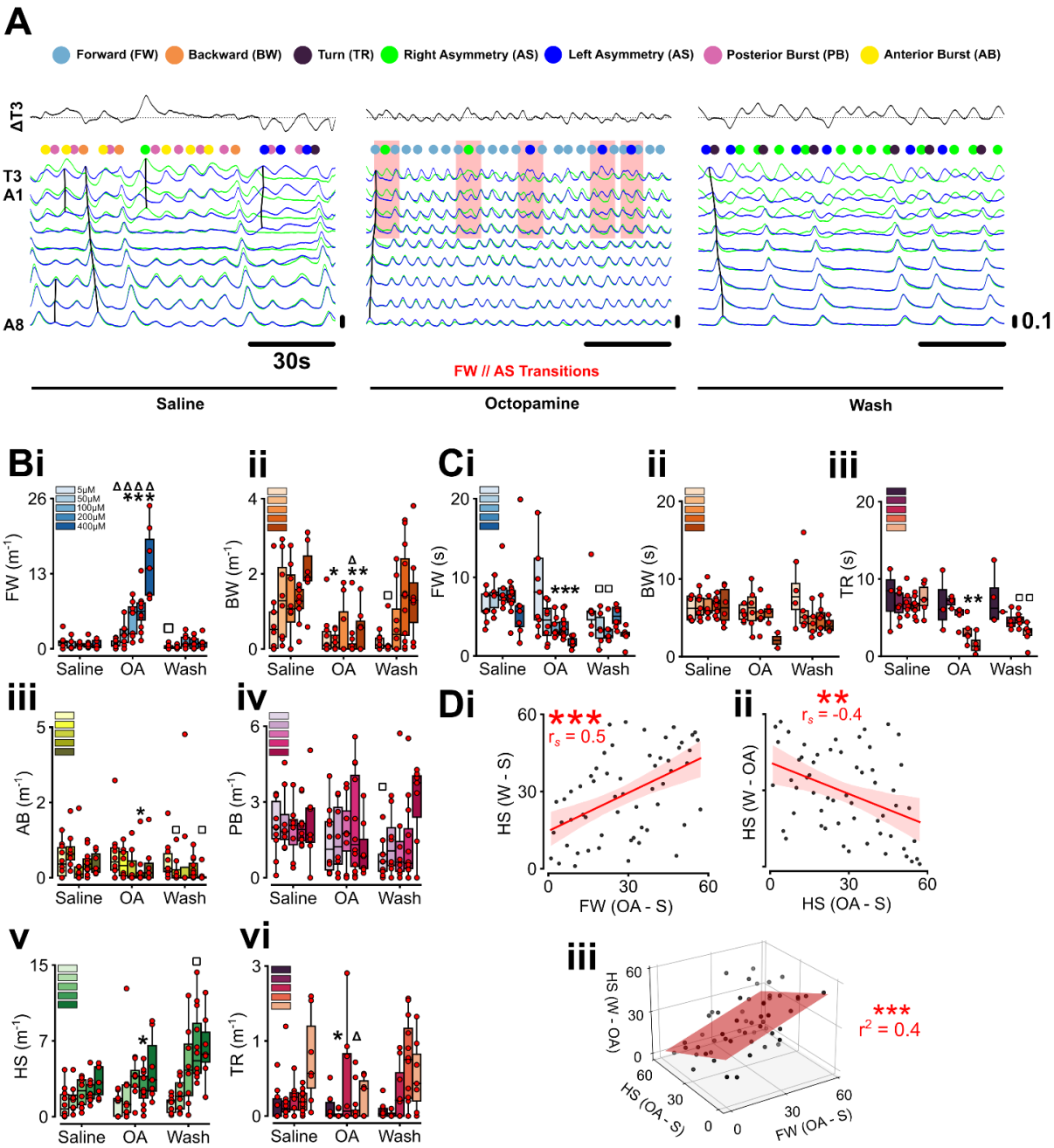

Figure 4: Bath Application of OA Induces Fictive Forward Bias in the isolated larval CNS

(**A**) Exemplar calcium dynamics in left (blue) and right (green) motor neurons in the 3rd instar isolated *Drosophila* ventral nerve cord (VNC) over 45 minutes under saline, octopamine (OA) (200μM), wash bath applications. Difference trace for T3 (ΔT3) shown above all traces (left - right). Dots above the traces indicate the initiation of the different fictive behaviours (light blue, fictive forward; orange, fictive backward; yellow, anterior symmetric burst; pink, posterior burst; blue, left anterior asymmetry; green, right anterior asymmetry). Black lines indicate the shape of each fictive activity to aid user's recognition of fictive programmes. Note that octopamine application induces fictive forward bias with intermittent asymmetric activity with the post-application wash period exhibiting dominating anterior asymmetric activity. (**B**) Changes in fictive frequencies of different fictive behaviours under the application of OA concentrations (5 - 400μM) between saline, OA perfusion, and wash conditions for fictive: (**i**) forward , (**ii**) backward, (**iii**) anterior burst, (**iv**) posterior burst, (**v**) anterior asymmetric headsweeps, and (**vi**) turn. Note that the axis showing the rate of each fictive activity is different for each fictive activity. (**C**) Activity propagation speed from

posterior (A8) to anterior (T3) for (**i**) fictive forward and anterior-to-posterior for (**ii**) fictive backward and (**iii**) fictive turning behaviours. (**D**) Ranked relationship between the relative effect of OA on promoting fictive forward activity and the relative change in headsweep asymmetric. (**Dii**) Ranked relationship between the relative promotion of anterior asymmetric activity by OA and the change in anterior asymmetric activity in wash relative to OA application activity level. (**Diii**) Ranked relationship between relative promotion of fictive forward waves by octopamine during application (X variable, FW (OA-S)), relative promotion of anterior asymmetric activity during octopamine application compared to the activity in the pre-application time window (Y variable, HS (OA-S)), and relative change in anterior asymmetric activity between the octopamine application and post-application time window (Z variable, HS (W-OA)). Z = 0.45*X + -0.44*Y + 27.78. Note the fact that fictive forward promotion in octopamine comes at the expense of asymmetric anterior headsweep activity. Significant post-hoc comparisons are exclusively shown denoted by ☐ saline vs wash, ✳saline vs OA, Δ OA vs wash.

Tyramine Bath Application Induces Fictive Overlap & Motor Competition

A pair of *tdc*$^{2+}$-expressing neurons in the T1 ganglion alongside descending neurons synthesise and release tyramine (TA) [7], [8], [10], [46]. Given the highly active coupling of intrinsic *tdc*$^{2+}$ activity and motor activity alongside OA's excitatory effect on fictive activity, we next evaluated the role of TA on CPG activity and motor competition. The outcome of TA modulation is considered oppositional to OA modulation with evidence of TA's inhibitory role on intact locomotion [27] and motor pool electrophysiology [34]. Thus, we turned to explore whether TA has a universal inhibitory role on motor competition in isolated preparations to better understand how behavioural inhibition manifests at a CPG and network level via *tdc*$^{2+}$ activity.

We explored the effect of TA by exogenously bath applying TA onto isolated 3rd instar larva VNC as in our OA experiments. Unlike OA, TA did not induce a consistent motor bias across applied concentrations compared to pre-application (Figure 5A, B). Across all fictive behavioural patterns, the only significant fictive changes occurred post-TA application. Specifically, fictive forward (200µM $0.6\pm0.4m^{-1}$ $p < .001$) and posterior burst (400µM $0.7\pm0.6m^{-1}$ $p < .001$) activity was significantly reduced in the wash period relative to the TA application period (FW, 200µM $10.3\pm8.1m^{-1}$) or pre-application saline period (PB, 200µM $18.7\pm11.5m^{-1}$) respectively. Further, again in contrast to OA, TA did not induce any significant changes to the intersegmental propagation of either fictive forward, backward, nor turn behaviours (Figure 5C). Reflective of this non-significant change in fictive incidences, TA perfusion appears to not induce significant, widespread changes in the landscape of fictive transitions (Supplementary Figure 5B). In fact, TA perfusion significantly increased the diversity of fictive transitions creating a less fictive biased network indicative of increased motor competition.

While TA did not induce fictive bias in the isolated network, TA perfusion induced a significant increase in the overlap of fictive motor programs (Figure 5A, Tyramine "Overlap") represented by wave activity commencing during the progression of a prior, incomplete fictive wave event. Perfusion of 200µM TA

514 induced a significant increase in time the network demonstrates activity overlap across at least one
515 segment (6.2±0.4% p = < .001) compared to the 0% overlap demonstrated during the pre-tyramine
516 application period (Figure 5D). Aside from overlap promotion, the application of ≥100µM TA induced
517 a significant decrease in the activity in the post-application in a concentration-dependent manner
518 (100µM 84.5±4.8% p = .01; 200µM 49.8±31.7% p = .002; 400µM 56.4±12.3% p = .006) compared to
519 pre-application period (100µM 95.4±3.8%; 200µM 93.2±9.8%; 400µM 97.7±2.2%) (Figure 5A, Wash
520 "Silence"; Figure 5Ei). Similar to our prior analysis evaluating correlations between fictive changes by
521 the OA and the post-application anterior asymmetric increase, we turned to correlation analysis
522 between the total time the isolated network executed fictive activity under TA versus the total time
523 where no fictive activity was demonstrated post-TA application to attempt to understand the long-
524 lasting modulatory effects of TA. However, we did not find any significant relationship between activity
525 changes by TA perfusion and the relative changes in activity in the post-application wash period (Figure
526 5Eii). Further, there was no significant relationship between the overlap and the post-application
527 silence promoted by TA (Figure 5Eiii). Given prior work has drawn attention to the state-dependent
528 effects of TA inhibition [26], we next evaluated if TA's effects on fictive activity were dependent upon
529 the activity state prior to TA application. As shown in Figure 5Eiv, TA did exhibit proportional and
530 increasing inhibitory effects as overall fictive activity levels rose beyond pre-application activity levels
531 > $6.7m^{-1}$ (p = .04, r^2 = 0.2). Thus, when baseline fictive activity is low, TA can have excitatory effects.
532 Taken together, TA promotes overlaps between different fictive motor programs and demonstrates
533 activity-dependent inhibition of overall fictive activity.

534 Given that previous work has indicated an inhibitory role for TA at an individual cellular level [26] [51],
535 we evaluated the effect of TA perfusion on motor nerve root bursting activity. Unexpectedly, TA
536 perfusion induced a positive, albeit non-significant, trend in motor root bursting (Supplementary
537 Figure 3Ai, ii) with no significant effects on bursting duration (Supplementary Figure 3Aiii), overall
538 duration of inactivity (Supplementary Figure 3Aiv), bursting amplitude (Supplementary Figure 3Av), or
539 tonic baseline amplitude (Supplementary Figure 3Avi). 200µM TA application induced a significant
540 reduction (p = .001) in the amplitude of calcium activity (Figure 3A, Supplementary Figure 3Bi, iii)
541 without, similar to OA, any changes to the baseline calcium activity (Supplementary Figure 3Bii, iv).

542 Overall, both neuromodulators – OA, TA – released by the *Drosophila* larval *tdc*$^{2+}$ system can
543 fundamentally reorient the fictive bias exhibited by the isolated network. While OA appears
544 consistently promotive to fictive rhythms engendering fictive forward bias, TA can be excitatory or
545 inhibitory on rhythm generation dependent on activity state. In effect, both neuromodulators have

complex neuromodulatory effects on fictive activity during and after their application which can be illuminated through considering their effects on expanding or constraining fictive motor diversity.

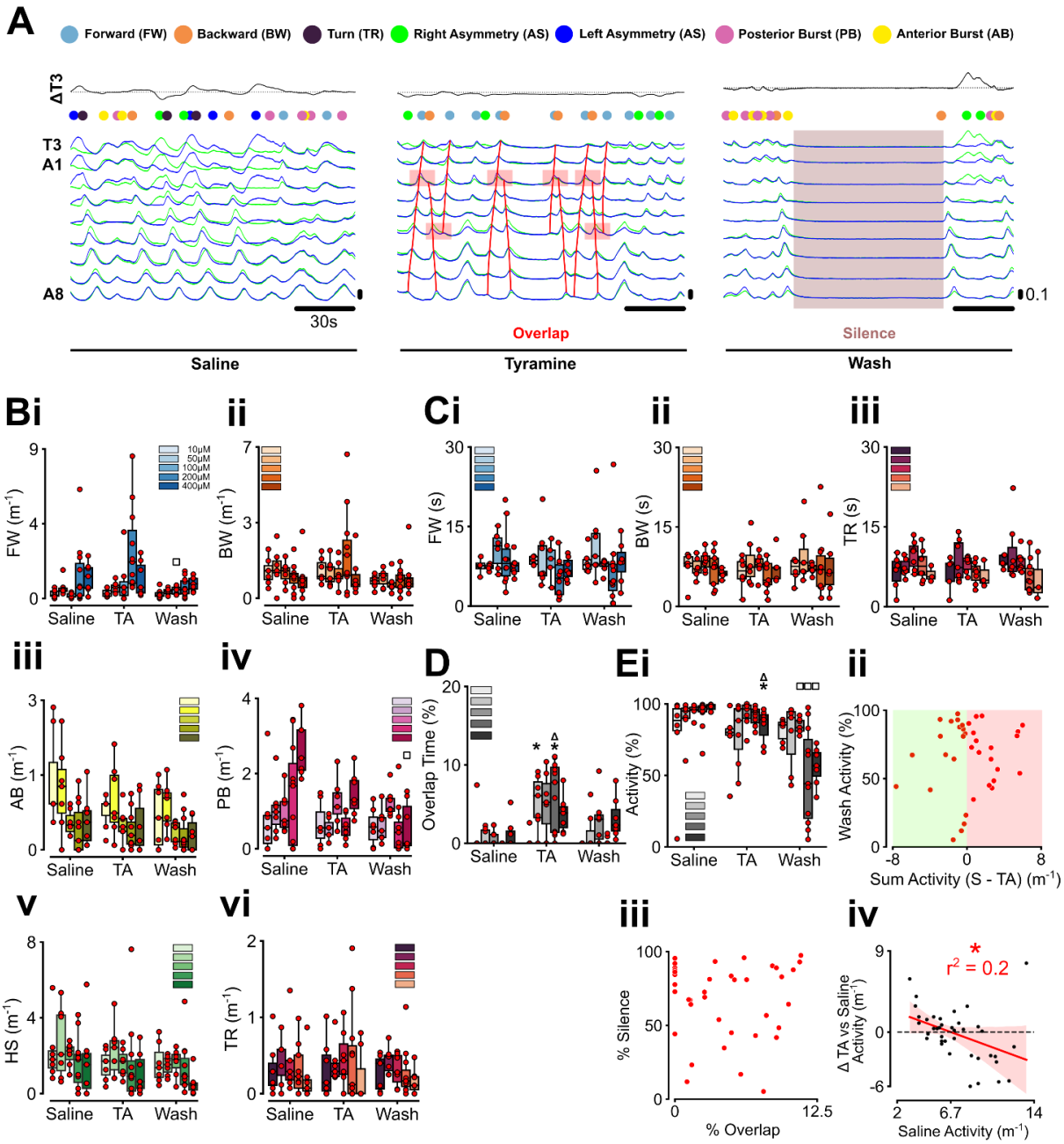

Figure 5: Bath Application of TA Induces Fictive Motor Overlap and Competition

(**A**) Exemplar calcium dynamics in left (blue) and right (green) motor neurons in the 3rd instar isolated *Drosophila* ventral nerve cord (VNC) over 45 minutes under saline, tyramine (TA) (200μM), wash bath applications. Note the overlap between fictive forward and backward motor activity (red) during tyramine application and absence of fictive activity in the wash period. (**B**) Changes in fictive frequencies of different fictive behaviours under the application of TA concentrations (10 - 400μM) between saline, TA perfusion, and wash conditions for fictive: (**i**) forward , (**ii**) backward, (**iii**) anterior burst, (**iv**) posterior burst, (**v**) anterior asymmetric headsweeps, and (**vi**) turn. Note that the axis showing the rate of each fictive activity is different for each fictive activity. (**C**) Activity propagation speed from posterior (A8) to anterior (T3) for (**i**) fictive forward and anterior-to-posterior for (**ii**) fictive backward and (**iii**) fictive turning behaviours. (**D**) Percentage of time where overlap in activity between segments exists for pre-application,

application, and post-application of TA across all concentration ranges. (**Ei**) Percentage of time where there is activity in at least one segment for pre-application, application, and post-application of TA across all concentration ranges. Note the concentration-dependent reduction in total activity within the wash period. (**Eii**) The effect of relative promotion (green) or suppression (red) of activity during TA application against the percentage of time where there is activity in at least one segment post TA application. Note the absence of a bifurcation or trend between wash activity and TA's promotive or suppressive activity relative to pre-application. (**Eiii**) Non-significant relationship between the % overlap induced by TA and post-application silence. (**Eiv**) The relationship between overall pre-application fictive activity ("Saline Activity") and the change in overall fictive activity during TA application ("TA vs Saline"). Note the activity-dependent inhibitory effect of tyramine. Significant post-hoc comparisons are exclusively shown denoted by □ saline vs wash, ✳saline vs TA, Δ TA vs wash.

Tdc^{2+} Neurons are Necessary and Sufficient for Fictive Locomotor Activity

Given the intrinsic *tdc*$^{2+}$ system is highly coupled to fictive activity and exogenous application of its neuromodulatory components can fundamentally alter motor diversity, we next evaluated if manipulating intrinsic *tdc*$^{2+}$ system activity can also alter motor competition. We expressed either *CsChrimson* or *GtACR1* in *tdc*$^{2+}$ neurons to optogenetically manipulate the intrinsic adrenergic-like system and evaluate motor neuron activity using nerve-root electrophysiology. Here, we show how intrinsic *tdc*$^{2+}$ activity is necessary and sufficient for fictive locomotor activity and exhibits most of the phenotypic effects displayed by exogenous OA application.

Firstly, we optogenetically depolarised *tdc*$^{2+}$ neurons by persistent red-light illumination (10, 20, 40s) and recorded motor root activity from T3 and A6 VNC ganglia (Figure 6A). Optogenetic depolarisation of *tdc*$^{2+}$ neurons induced significantly increased motor root bursting for all: 10s (pre: 9.6$\pm$7.5 m^{-1}, on: 55.4$\pm$26.1 m^{-1}, p = .002), 20s (pre: 11.4$\pm$4.6 m^{-1}, on: 46.3$\pm$9.1 m^{-1}, p=.002), and 40s (pre: 11.2$\pm$6.6 m^{-1}, on: 41.0$\pm$12.9 m^{-1}, p=.005) stimulation periods (Figure 6A, Ci). The increased bursting frequency in A6 was accompanied by significant decrease in bursting duration for all: 10s (pre: 2.8$\pm$1.3 m^{-1}, on: 1.0$\pm$0.4 m^{-1}, p=.002) 20s (pre: 3.3$\pm$1.2 m^{-1}, on: 0.9$\pm$0.3 m^{-1}, p=.004), and 40s (pre: 3.2$\pm$1.7 m^{-1}, on: 1.7$\pm$1.9 m^{-1}, p=.005) stimulation periods (Figure 6Cii). Elevated A6 motor root bursting frequency was also evocable by pulsed-based stimulation (Supplementary Figure 4). Across both continuous and pulsed-based stimulation of *tdc*$^{2+}$ neurons, intrinsic manipulation of the *tdc*$^{2+}$ system induced fictive forward bias akin to results demonstrated by exogenous OA application (Figure 6E). Specifically, optogenetic depolarisation of *tdc*$^{2+}$ neurons induced significantly increased fictive forward motor bias for all: 10s (pre: 3.3$\pm$2.2 m^{-1}, on: 64.2$\pm$43.0 m^{-1}, p < .001), 20s (pre: 4.3$\pm$4.0 m^{-1}, on: 36.3$\pm$7.7 m^{-1}, p < .001), and 40s (pre: 4.8$\pm$5.1 m^{-1}, on: 36.8$\pm$10.8 m^{-1}, p <.001) stimulation periods. In terms of fictive bias, averaged across stimulation periods, optogenetic depolarisation of *tdc*$^{2+}$ neurons induced fictive forward waves to become 79$\pm$8% of all fictive activity events during stimulation as opposed to 36$\pm$13% before or 36$\pm$14% after red-light stimulation.

Counter to the relationship found between promoted fictive forward and anterior asymmetric elevated activity in exogenous octopamine application, anterior asymmetric fictive activity was not elevated in the post-stimulation relative to pre-stimulation period (Figure 6F). Further, while we witnessed a consistent elevation in silence (i.e., continuous lack of apparent rhythmic activity in any nerve root) post optogenetic stimulation (see Figure 6A, ~40s post-stimulation, 34.6$\pm$27.8 m) compared to control preparations (9.9$\pm$9.1 m), the duration of silence did not significantly differ ($p = .58$) nor covary with stimulation period (10s: $p = .07$; 20s: $p = .27$; 40s: $p = .25$) (Figure 4G). Thus, depolarising *tdc*$^{2+}$ neurons is sufficient to induce the main fictive biasing effects witnessed by OA exogenous application.

Secondly, we optogenetically hyperpolarised *tdc*$^{2+}$ neurons with pulses of light (15s, 30s, 60s) and recorded motor root activity from T3 and A6 VNC ganglia (Figure 6B). Optogenetic hyperpolarisation of *tdc*$^{2+}$ neurons significantly reduced, and in many cases, completely collapsed, motor root bursting for all light-stimulation periods: 15s (pre: 1.6$\pm$2.1 m^{-1}, on: 0.5$\pm$1 m^{-1}, $p = .04$), 30s (pre: 1.8$\pm$1.8 m^{-1}, on: 0$\pm$0 m^{-1}, $p=.009$), and 60s (pre: 2.2$\pm$2.1 m^{-1}, on: 0.4$\pm$0.7 m^{-1}, $p = .01$) illumination periods with 37 of 49 (75.9$\pm$30.8%) trials across preparations (N=7) showing no fictive activity during the white-light stimulation period (Figure 6Bii, D). For longer period white-light stimulation (> 15s), there was weak recovery of rhythmic activity in the A6, indicative of post-inhibitory rebound. Interestingly, long-lasting (60s) LED white-light illumination in *tdc*$^{2+}$*>GtACR1* no retinol control preparations induced significantly increased (pre: 1.8$\pm$2.0 m^{-1}, on: 3.7$\pm$1.5 m^{-1}, $p = .01$) A6 motor root activity potentially indicative of photoreceptor-based motor stimulation in the isolated VNC preparation.

Thus, *tdc*$^{2+}$ depolarisation provokes elevated fictive forward activity akin to exogenous OA application. Further, *tdc*$^{2+}$ hyperpolarisation collapsed all motor rhythms. Considering the strong correlation between intrinsic *tdc*$^{2+}$ and motor neuron activity, such results demonstrate *tdc*$^{2+}$ neurons are necessary and sufficient for fictive motor activity in isolated VNC 3rd *Drosophila* larval preparations.

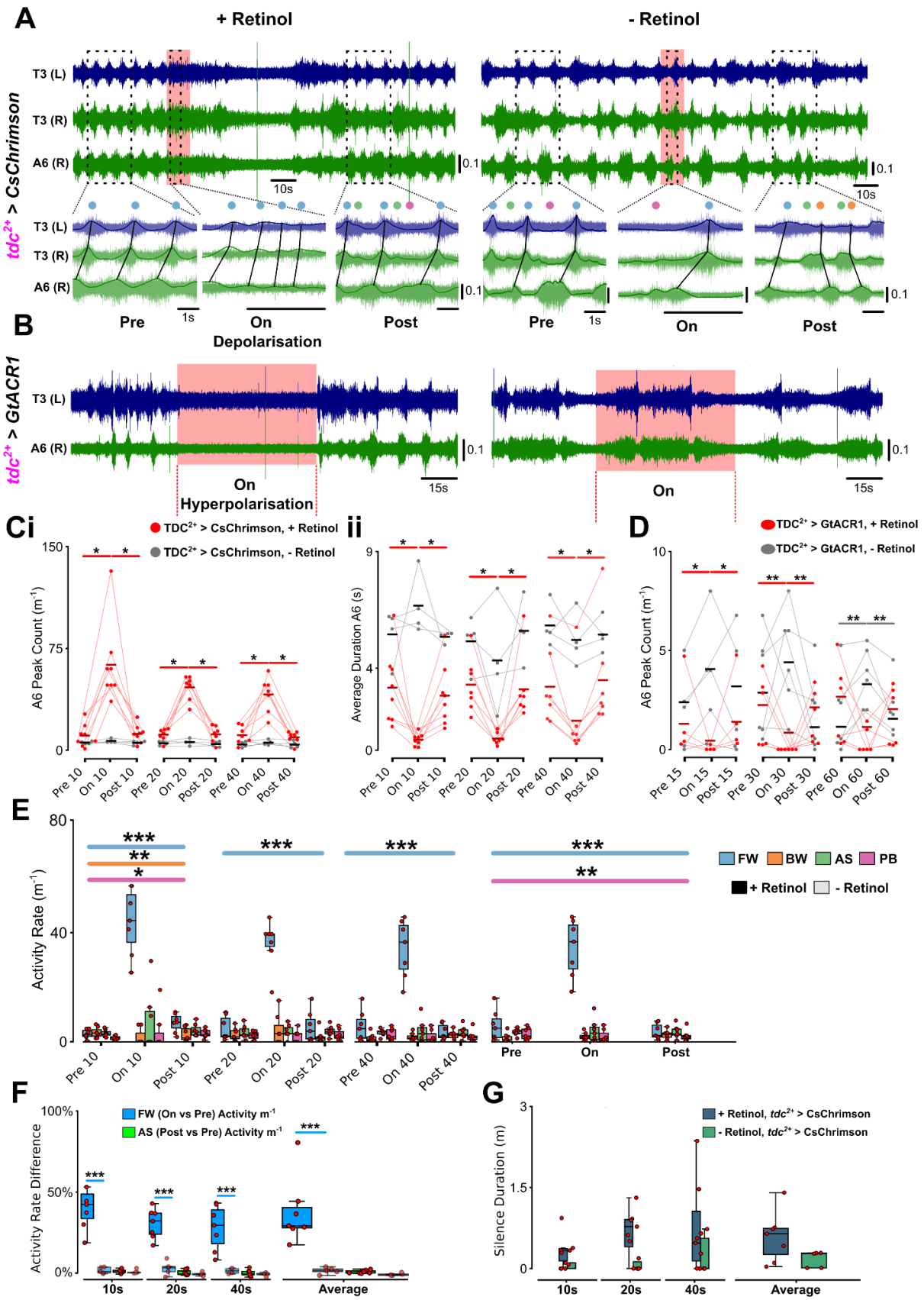

Figure 6: *tdc*$^{2+}$ Neuronal Activity is Sufficient and Necessary for Fictive Locomotor Activity

(**A**) Exemplar three nerve root (T3 (L), T3 (R), A6(R)) electrophysiology trace for continuous red-light depolarisation of *tdc*$^{2+}$ neurons using CsChrimson for preparations raised on retinol (experimental, left) and no retinol (control,

right). Before, during (red box), and post-stimulation periods are shown with rectified and smoothed traces shown. Black lines represent fictive activity motifs. (**B**) Exemplar two nerve root (T3 (L), A6 (R)) electrophysiology trace for continuous white-light hyperpolarisation (red box) of *tdc*$^{2+}$ neurons using GtACR1 for preparations raised on retinol (experimental, left), and no retinol (control, right). (**C**) Quantification of abdominal (A6) motor root bursting for (**i**) burst rate and (**ii**) duration of bursts in *tdc*$^{2+}$>CsChrimson for 10s, 20s, and 40s depolarisation period. (**D**) Quantification of abdominal (A6) motor root bursting for burst rate in *tdc*$^{2+}$>GtACR1 for 15s, 30s, and 60s hyperpolarisation period. (**E**) Change in the fictive activity profile for *tdc*$^{2+}$>CsChrimson stimulation periods demonstrating inducing of fictive forward bias across stimulation period. Activity profile within stimulation periods and average across stimulation periods are shown. (**F**) Difference in activity rate of fictive forward activity between stimulation and pre-stimulation period (blue) as well as fictive anterior asymmetric activity between post-stimulation and pre-stimulation period (green). (**G**) Duration of no rhythmic activity quantified post stimulation periods in control (- retinol) and experimental (+ retinol, CsChrimson) preparations. Comparisons followed by post-hoc was conducted with p-values: < .5 (*), < .01 (**), <.001 (***) shown. Only statistically significant bars are shown.

Given the *tdc*$^{2+}$ neuron population consists of local and projecting neurons, we next turned to spatially-restricting depolarisation to exclusively *tdc*$^{2+}$ VNC neurons to assess the effect of VNC octopaminergic neuron modulation of fictive locomotion. To evaluate any effect of spatially-restricted release of OA on fictive locomotion, we performed restricted red-light stimulation on *tdc*$^{2+}$ neuronal populations in the ventromedial axis on the isolated ventral nerve cord. Qualitatively, direct red-light stimulation of *tdc*$^{2+}$ neuronal populations induces elevated bursting rate in all restricted regions: SOG (Figure 7A), thoracic ganglion (Figure 7B), anterior abdominal ganglion (Figure 7C), and posterior abdominal ganglion (Figure 7D). Across all stimulation regions, both the thoracic and abdominal nerve root bursting rate is significantly increased during *tdc*$^{2+}$ depolarisation (Figure 8Ai - Di). Specifically, direct SOG *tdc*$^{2+}$ depolarisation induced a significant increase in T3 (pre: 8.3$\pm$4.8 m^{-1}, on: 30.0$\pm$6.9 m^{-1}, p = .001) and A6 (pre: 8.8$\pm$4.7 m^{-1}, on: 31.7$\pm$10.8 m^{-1}, p = .001) motor root burst rate (Figure 8Ai). Direct thoracic ganglion (T1-3) *tdc*$^{2+}$ depolarisation induced a significant increase in T3 (pre: 6.5$\pm$3.4 m^{-1}, on: 30.0$\pm$6.0 m^{-1}, p < .001) and A6 (pre: 6.8$\pm$3.5 m^{-1}, on: 37.7$\pm$13.3 m^{-1}, p < .001) motor root burst rate (Figure 6Bi). Direct anterior abdominal ganglion (A1-3) *tdc*$^{2+}$ depolarisation induced a significant increase in T3 (pre: 6.6$\pm$2.1 m^{-1}, on: 34.3$\pm$12.4 m^{-1}, p = .001) and A6 (pre: 6.8$\pm$3.5 m^{-1}, on: 32.6$\pm$17.3 m^{-1}, p = .022) motor root burst rate (Figure 8Ci). Finally, direct posterior abdominal ganglion (A6-8) *tdc*$^{2+}$ depolarisation induced a significant increase in T3 (pre: 6.1$\pm$2.5 m^{-1}, on: 48.0$\pm$12.0 m^{-1}, p < .001) and A6 (pre: 6.5$\pm$2.1 m^{-1}, on: 45.4$\pm$9.7 m^{-1}, p < .001) motor root burst rate (Figure 8Di). Further, across all stimulation regions, both the thoracic and abdominal nerve root bursting duration was significantly reduced during *tdc*$^{2+}$ depolarisation with the exception of the T3 motor root during thoracic and anterior abdominal ganglion (Figure 8Ai-Di). Specifically, direct SOG *tdc*$^{2+}$ depolarisation induced a significant decrease in T3 (pre: 3.0$\pm$1.3s, on: 1.5$\pm$0.6s, p = .01) and A6 (pre: 3.0$\pm$1.3s, on: 1.3$\pm$0.4s, p = .03) motor root burst duration (Figure 8Ai). While direct thoracic ganglion (T1-3) *tdc*$^{2+}$ depolarisation did not induced a significant decrease in T3 motor root burst rate (pre: 2.9$\pm$1.0s, on:

659 1.5±0.4s, p = n.s), depolarisation of T1-T3 *tdc*$^{2+}$ neurons did induce a significant decrease in the A6
660 motor root burst duration (pre: 3.1±1.9s, on: 1.4±0.6s, p = .02) (Figure 8Bi). While direct anterior
661 abdominal ganglion (A1-3) *tdc*$^{2+}$ depolarisation did not induced a significant decrease in T3 motor root
662 burst rate (pre: 3.2±1.2s, on: 1.5±0.4 m^{-1}, p = n.s), depolarisation of A1-A3 *tdc*$^{2+}$ neuron did induce a
663 significant decrease in the A6 motor root burst duration (pre: 3.1±1.9s, on: 1.4±0.6s, p = .04) (Figure
664 8Ci). Finally, direct posterior abdominal ganglion (A6-8) *tdc*$^{2+}$ depolarisation induced a significant
665 decrease in T3 (pre: 3.5±1.3s, on: 1.1±0.2s, p = .001) and A6 (pre: 3.3±1.1s, on: 1.1±0.2s, p = .003)
666 motor root burst duration (Figure 8Di). Thus, depolarisation of any ganglion *tdc*$^{2+}$ neuron
667 subpopulation is sufficient to induce elevated motor activity in the isolated ventral nerve curve.

668 We next examined if sub-region restricted *tdc*$^{2+}$ neuron depolarisation induced fictive forward bias
669 akin to our earlier results on exogenous OA application and whole-VNC *tdc*$^{2+}$ depolarisation.
670 Depolarisation of *tdc*$^{2+}$ neurons in the SOG (Figure 8Aii), thoracic ganglion (Figure 8Bii) and anterior
671 abdominal ganglion (Figure 8Cii) induced a non-significant elevated mixture of fictive behavioural
672 patterns. However, decomposing the population data down into individual iterations of restricted
673 stimulation across preparations did demonstrate a significant variation in the fictive bias within each
674 region of *tdc*$^{2+}$ depolarisation (Supplementary Figure 5). Namely, restricted *tdc*$^{2+}$ depolarisation in the
675 SOG (Supplementary Figure 5A, $\chi^2(2) = 7.3$, p = .007), thoracic ganglion (Supplementary Figure 5B, $\chi^2(2)$
676 = 7.3, p = .007), and anterior abdominal ganglion (Supplementary Figure 5C, $\chi^2(2) = 7.3$, p = .007) all
677 significant induced changes in fictive wave bias with some instances showing promotion of fictive
678 forward whereas others fictive backward bias. In other words, while averaging between preparations
679 demonstrates a general trend of promoting both fictive forward and backward preparation in
680 restricted *tdc*$^{2+}$ depolarisation in the SOG, T1-3, and A1-3, in individual trials, there are many instances
681 of either fictive forward or backward bias resultants. In contrast, posterior abdominal restricted *tdc*$^{2+}$
682 depolarisation induced a significant increase in exclusively fictive forward motor activity (pre:
683 2.4±1.9m^{-1}, on: 38.6±13.8m^{-1}, p = .005) (Figure 8Dii). While posterior abdominal restricted *tdc*$^{2+}$
684 depolarisation similarly induced increased fictive bias variation (Supplementary Figure 5D, $\chi^2(2) = 5.8$,
685 p = .02), a majority of stimulation instances were fictive forward biased. Thus, both abdominal
686 posterior and whole *tdc*$^{2+}$ depolarisation induced locomotor CPGs into a fictive forward bias.

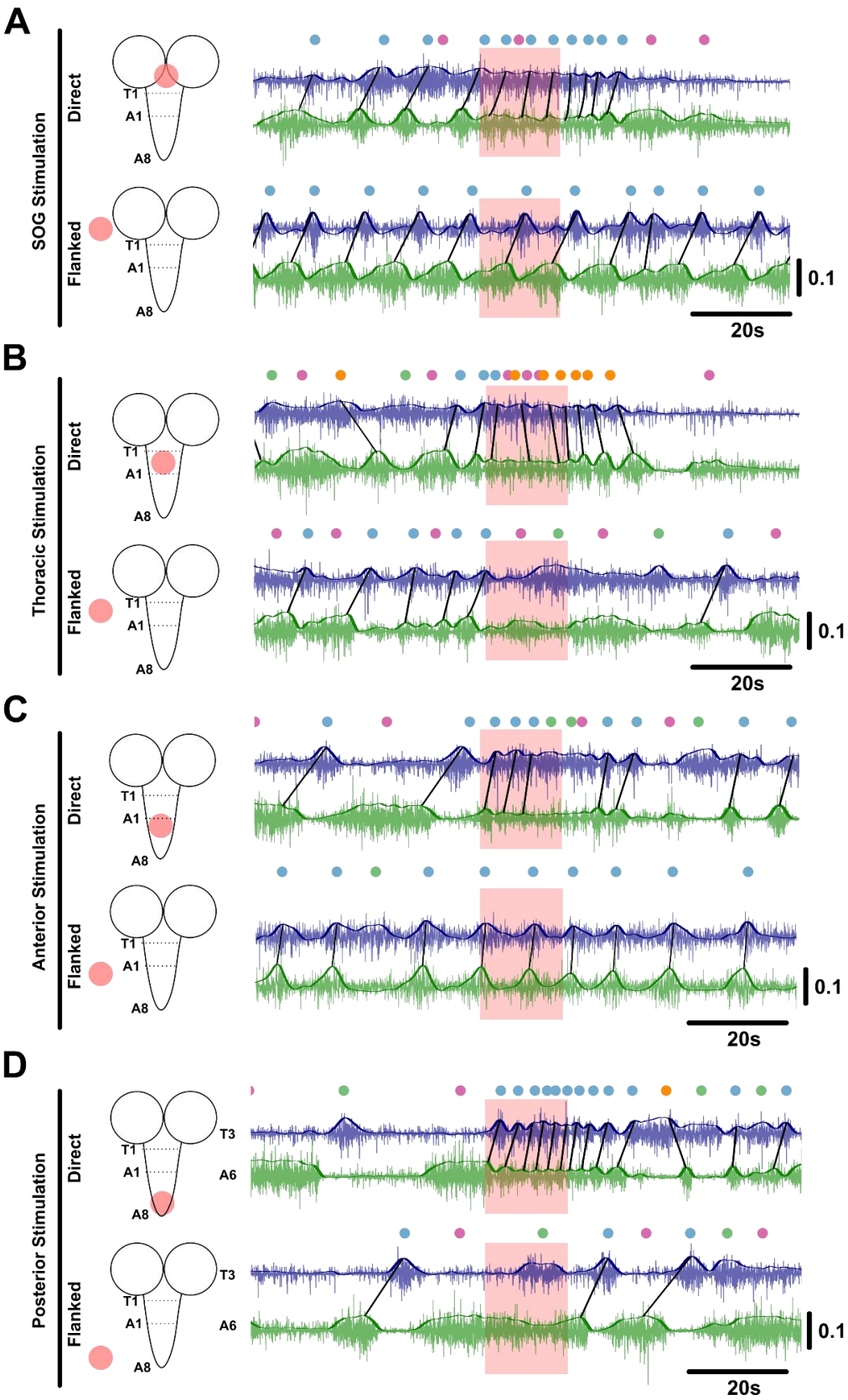

Figure 7: Restricted Optogenetic Stimulation of *tdc*$^{2+}$ Neurons Induces Diversity of Activity

Restricted 10s optogenetic stimulation of *tdc2+* neurons in the (**A**) SOG, (**B**) thoracic ganglion (T1-T3), (**C**) anterior abdominal ganglion (A1-A3), and (**D**) posterior abdominal ganglion (A6-A8). Representative electrophysiology

thoracic (T3) and posterior abdominal (A6) nerve root recording traces for direct and flanked stimulation conditions shown with coloured-dots indicating occurrence of fictive motor pattern: fictive forward wave (blue dot), posterior burst (purple dot), fictive backward wave (orange dot), anterior a/symmetric activity (green dot).

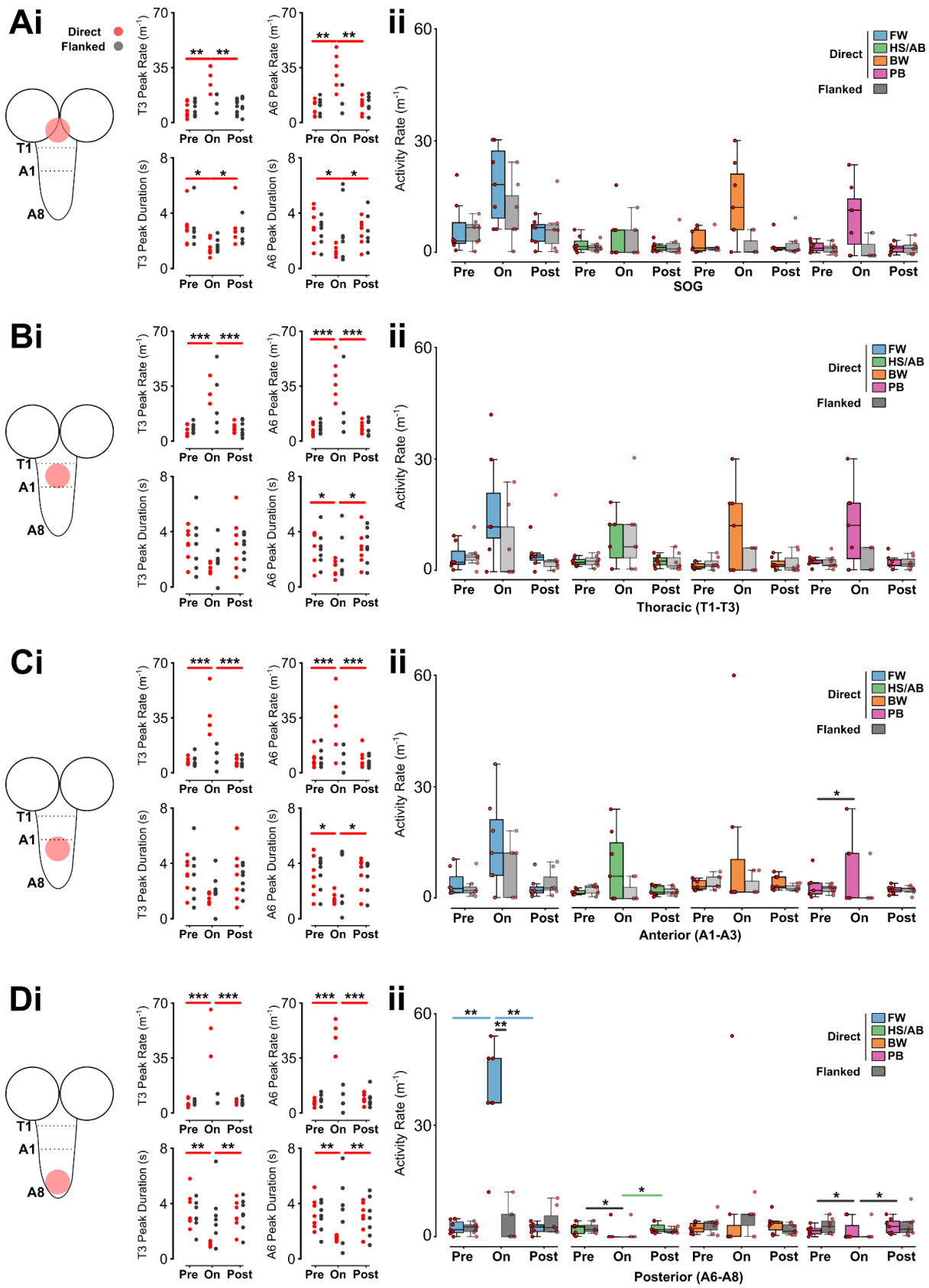

Figure 8: Optogenetic Stimulation of Posterior Abdominal *tdc*$^{2+}$ Neurons Induces Fictive Forward Locomotion

Quantification of (**i**) abdominal and thoracic burst rate, burst duration, and (**ii**) fictive activity ("FW" = fictive forward wave, "HS/AB" = anterior symmetric or asymmetric, "BW" = fictive backward wave, "PB" = posterior bust) rate during direct (colour) and flanked (grey) optogenetic stimulation of (**A**) SOG, (**B**) thoracic ganglion (T1-T3), (**C**) anterior abdominal ganglion (A1-A3), and (**D**) posterior abdominal ganglion (A6-A8) *tdc*$^{2+}$ neurons. Comparisons followed by post-hoc was conducted with p-values: < .5 (*), < .01 (**), <.001 (***) shown. Only statistically significant bars are shown.

Discussion

The adrenergic-like system is involved in a diversity of behaviours across invertebrates. Here, we show that the adrenergic-like *tdc*$^{2+}$ system is necessary and sufficient for generating rhythmic activity in *Drosophila* larval CPG networks. Through acute manipulations to OA and TA signalling, we demonstrate that these core adrenergic-like neuromodulators may not always be oppositional for locomotion in *Drosophila* larvae at the isolated network level. Finally, we discovered that a by-product of extensive and sustained motor bias is an instantiation of alternate fictive activity after the end of a prior bias episode. A crucial element of sustained movement is action selection and the inhibition of those competing motor programs that induce different locomotion (e.g., forwards vs backwards). Here, we show how the isolated neural system appears to have an innate disposition to rebalance motor diversity by potentiating alternative motor patterns in response to suppression of motor diversity through sustained motor bias.

The Fundamental Role of *Tdc*$^{2+}$ Activity in *Drosophila* Larvae Fictive Activity

The effects of exogenous application of octopamine (OA) and tyramine (TA) onto isolated preparations mirror the effects of genetic ablation and manipulations within intact animals. Specifically, elevation of TA levels either through TβH mutant *Drosophila* larva [27], [48] or feeding [34] induces dysrhythmic movement manifesting as slower movement with more pauses. Indeed, the inhibitory effects of tyramine are common to other invertebrates like *C. elegans* [33], [52]. Interestingly, here we showed exogenous TA application does not immediately induce pausing in activity but instead the induction of overlaps in fictive programs implying dysrhythmic, slower locomotion in intact *Drosophila* may not be a product of slower rhythm generation but incomplete motor generation that reduces movement speed and distance. In contrast, elevation of OA levels via direct application [4], [18], [63] or starvation [21], [24] are generally promotive of movement. Here, we found octopamine similarly induced elevated, fasting fictive forward rhythms in line with behavioural studies. However, we found the sustained forward bias induced by octopamine endangered long-lasting anterior asymmetric activity post application currently not exhibited in intact animal behaviour. In future, *Drosophila* behavioural

studies could look at the long-lasting effects of sustained motor bias through acute manipulations as reported here.

Prior studies have shown how genetic manipulations to the adrenergic-like system in a variety of invertebrates induces dysrhythmic movement in intact, free-moving animals [4], [9], [27], [28]. Leaving aside potentially developmental compensatory effects, the fact that genetic ablation of the *tdc*$^{2+}$ system does not arrest all movement in intact animals [33], whereas our results on *tdc*$^{2+}$ system hyperpolarisation in isolated networks do collapse rhythmic generation, implies re-afferent, compensatory adaptability in other neuromodulatory systems or sensory modulation may be sources of compensation in intact animals with dysfunctional *tdc*$^{2+}$ systems. In the future, the genetic manipulations could be performed acutely on the isolated CNS preparation to interrogate how widespread *tdc*$^{2+}$ system deficits manifest at a neural level to further bridge our understanding between intact and fictive locomotion.

Modelling Constraints for a *Tdc*$^{2+}$-Motor System Model

While the cellular architecture of adrenergic-like *tdc*$^{2+}$ system in *Drosophila* is reported [48], [64], the essentiality of the system for motor output is underexplored. Here, we showed key features of exogenous and intrinsic adrenergic-like modulation that may constrain future connectome-based modelling of motor system architecture.

Despite the absence of a comprehensive list of specific presynaptic partners for the *tdc*$^{2+}$ system, we can infer that the *tdc*$^{2+}$ system likely exists directly upstream of the VNC rhythm generating networks. Based on current connectomics data, only the ascending and descending subparts of the *Drosophila* 1st instar larva *tdc*$^{2+}$ system appear to have postsynaptic partners. The VNC *tdc*$^{2+}$ system appears to exclusively project to the neuromuscular junction [48], [64], [65]. Given the high correlation in *tdc*$^{2+}$ system activity to system-wide segmental motor activity alongside the fact that hyperpolarisation of the *tdc*$^{2+}$ system evoked an immediate cessation of fictive activity, our results imply the *tdc*$^{2+}$ system may have a direct neuromodulatory roles that might emerge after the 1st instar developmental stage. The complete connectome and architectural makeup of the 3rd instar *Drosophila* larvae is undetermined; one testable prediction is that segmental *tdc*$^{2+}$ neuronal populations are connected, directly or indirectly, to reported GDL/A27h premotor circuity, or intermediary accessory of descending command neuronal structures like MDN, and Pair1 interneurons [66], [67], [68]. Further, the *tdc*$^{2+}$ system may make direct synaptic connections to pacemaker command neurons (i.e., AcN, A01j) underpinning locomotory speed [69]. Indeed, such predictions are supported by the tyraminergic architecture in *C. elegans* wherein the activity of RIM neurons - presynaptic to GABAergic

premotor neurons that facilitate bending - occurs prior to changes in motor neuron activity [33], [51], [52], [53], [54]. Further, the highly coordinated and rhythmic behaviour of the *tdc*$^{2+}$ system itself implies the existence of a similar intersegmental regulatory architecture which may include GDL-like feedforward inhibitory motifs [64]. Importantly, the *tdc*$^{2+}$-GAL4 construct also incorporates large ventral unpaired median (VUM) motor neurons - a subset of the *tdc*$^{2+}$ system and motor neurons system - that appear to exclusively innervate the larval muscles [66]. While hyperpolarizing these neurons should undoubtedly reduce motor pool activity, the fact that system-wide motor activity comprehensively collapses under mass hyperpolarisation suggests still a fundamental role of the interneuronal or descending portions of the *tdc*$^{2+}$ system in fictive rhythmic generation. Consequently, we might expect any realised or modelled architecture of the *tdc*$^{2+}$ system to incorporate a subpopulation motif for both internal and projecting outputs. Finally, independent of architecture, the mechanism of modulation by the *tdc*$^{2+}$ system may be more complex than simply adrenergic-like modulation by OA and TA exclusively. Indeed, we have only a partial OA/TA receptor expression map restricted to the tissue, but not cellular level [4], [6], [70], [71]. Given that different OA/TA receptor isoforms have fundamentally different downstream signalling effects [4] and thus different effects on behaviour (e.g., [22]), any neuromodulatory mechanistic picture currently lacks a firm foundation. Further, given a majority of adult *tdc*$^{2+}$ neurons co-express OA and glutamate [72] and some *tdc*$^{2+}$ neurons modulate through gap junctions (e.g., APL neurons in the MB [73]), a complex, potentially degenerate, neuromodulatory picture may underpin the mechanism behind *tdc*$^{2+}$ system fictive modulation. Overall, we show that the *tdc*$^{2+}$ system could be considered at least part of a necessary and sufficient motif for rhythm generation in locomotory networks.

The Adrenergic-like System in Modulating Motor Competition

Movement necessitates a balance between excitation-driven initiation of a rhythm and pattern generating circuit alongside inhibition of competing motor program-related networks. Motor competition - the dynamic interplay that underpins excitatory and inhibitory neural action - is one lens through which the OA/TA modulatory dichotomy has yet to be examined. Here, we demonstrated that the well-reported excitatory role of OA and the inhibitory role of TA can be considered as neuromodulators underpinning motor network competition.

The locomotor effects of OA/TA neuromodulation are well-reported across a variety of invertebrate species. Generally, the OA/TA are considered mutual-antagonistic in locomotor neuromodulation with an excitatory/inhibitory binary [4], [26]. Complementing some studies that highlighted nuanced roles for adrenergic-like neuromodulation [26], we showed that TA exhibited activity-dependent inhibitory effects, was promotive of overlapping between fictive programs, thus not exclusively leading to

794 inhibitory effects. Thus, the slower and shorter locomotion exhibited when *Drosophila* larva are fed
795 TA [27] could be conceived as a failure to regulate motor competition rather than a direct, general
796 inhibitory effect. Those two competing explanations for TA effects are non-trivial differences. For
797 instance, while TA has a hyperpolarising effect on an isolated neuron [34] ,we found an overall trend
798 of TA to depolarise motor pool activity. Our indication that TA's inhibitory effects may be a product of
799 activity state can help marry the two bodies of thought. Namely, given that intrinsic tdc^{2+} activity is
800 highly coupled to fictive motor activity, tdc^{2+} activity is indicative of OA release [48], and that TA's
801 effects might be conditional on OA levels [26], one can see how TA/OA's antagonism is in response to
802 their neuromodulatory effects. At a functional level, we therefore could consider OA/TA as mutual-
803 antagonists altering motor competition rather than generally activity levels.

804 Our results and the role of the tdc^{2+} system in *Drosophila* larvae can be greatly contextualised by its
805 similarity to the *C. elegans* neuroarchitecture underpinning turning escape behaviour. Within *C.*
806 *elegans*, OA/TA play a significant and fundamental role in modulating escape behaviour and motor
807 competition through the AVA/AVB/RIM motif [26], [53]. Importantly, the proposed motif
808 demonstrates how TA/OA underpins motor competition between spontaneous forward and backward
809 locomotion through TA's disinhibition [54]. Taken together with the effect of increased overlap and
810 activity-dependent inhibition within our work, we could expect TA to have a similar disinhibitory role
811 in *Drosophila*. Namely, as reported in our recent work [1], core interneuronal inhibitory motifs might
812 be essential for all forms of motor selection and appropriate rhythmic output. Thus, we would expect
813 the tdc^{2+} system - itself releasing neuromodulators essential for escape responses - to be integral to
814 orchestrating and modulating the dynamics of motor selection at a fundamental level.
815
816 OA's excitatory effect on fictive motor behaviour is reflective of an underlying inhibition of motor
817 competition. Reminiscent of a large catalogue of prior studies [3], [8], [9], [26], [27], [32], we found
818 exogenously-applied OA was excitatory by being promotive of forward fictive locomotion with higher
819 intersegmental propagation of activity. Importantly, this promotion of locomotion, especially given
820 the network appeared perpetually active with little to no episodes of non-activity, was reflective of
821 significant inhibition of competing motor program occurrence. Indicative of a suppression of initiation,
822 we here contextualise the neuromodulator OA, in comparison to TA, as a suppressor of motor
823 competition. Reflective of a deeper role of the adrenergic-like system in motor competition, the
824 emergence of proportional post-application activity changes due to OA's neuromodulatory effects
825 indicates a potential foundational connection in CPG competition. Given that asymmetric anterior
826 activity can be considered a preliminary and important element of backward locomotion [1], the fact
827 OA's induction of an exclusive fictive forward bias precipitated an elevation of such asymmetric

anterior activity post-hoc suggests a potential underpinning dynamic in motor selection. Namely, a long-lasting memory-like system may exist to compensate for extremes in fictive forward activity that compensates if that extreme bias manifests. Indeed, the emergence of post-application elevation in silence from TA perfusion may also be reflective of a long-lasting effect to motor competition promotion. Unsurprisingly, inhibition is a vital element in necessitating variability as for a system to be able to devolve into different output modes it must first have a configuration that allows it to sit at that potential junction (i.e., conception of criticality) [1], [74]. Notably, there was no apparent post-asymmetric elevation in our electrophysiology-based stimulation as exhibited in our exogenous perfusion data. Thus, we would predict "long-lasting bias" could be denoted within a motor system as dominance of one fictive motif beyond a 60s episode.

Taken together, here we provide a case of how the *tdc*$^{2+}$ system in *Drosophila* may be a necessary and sufficient component in rhythm generation underlying locomotion. Further, we nuance the role of adrenergic-like neuromodulation in motor competition by demonstrating how OA/TA operate to either restrain or promote diversity of fictive motor programmes. Our results provide constraints on modelling studies and a framework for further connectomics exploration into how the *tdc*$^{2+}$ activity is integrated into the pre-motor system. Finally, we highlight a novel potential relationship within motor competition between induced locomotion bias and long-lasting fictive antagonism that may demonstrate a fundamental relationship of CPG networks not currently considered.

Conceptualising Neuromodulation of Motor Competition and Criticality

Ensuring appropriate movement is logically achievable by potentiating motor networks to be able to output a diverse range of motor patters while restraining unnecessary bias towards one motor program. At a fundamental level, this dynamic interplay between differentially excitation and inhibition where different CPG networks are competing for a winner-takes-all-like output we defined here as motor competition. The conceptualisation of network dynamics, competition between outputs, and the underlying dynamic interplay between excitation and inhibition as a source of output variability is well-document in modelling and examinations of cortical network dynamics [75], [76], [77], [78]. An alternative way of conceptualising the motor competition discussed here is through the concept of criticality [79], [80]. A network primed for adaptive output diversity ought to be in a state of being able to transition to any individual type of output pattern within its range of potential outputs – a state of criticality. For locomotory networks, being at a state of criticality would be ensuring the network is capable of transition to any fictive activity pattern or motif sequences when driven to by afferent or intrinsic drives. Given neuromodulation is fundamentally about reorientating network

output, here, we begin to examine adrenergic-like neuromodulation through the lens of motor competition and criticality.

Exogenous adrenergic-like manipulations and intrinsic *tdc*$^{2+}$ system manipulations reoriented the network away from producing a diversity of fictive motor programs into a restrictive fictive state: the effect of sustained neuromodulation pushed the isolated locomotory network from a state of putative criticality into a biased state. For OA application, the engendering of a fictive forward bias state resulted in an anterior asymmetric state before return to baseline fictive diversity. For TA application, the induction of overlapping fictive behaviours – conceptualizable as a breakdown in the inhibition between motor program initiation and thus increased unrestrained motor competition – induced bouts of no activity before return to baseline fictive diversity. Thus, each neuromodulatory effect reveals potential different recovery pathways from sustained bias back to a critical state. Thus, we showed how neuromodulatory application and manipulation of the *tdc*$^{2+}$ system are first-basis tools for manipulating motor competition. Indeed, through our acute manipulations, we found some indication of reorientation effects (e.g., anterior asymmetric promotion after OA-induced forward bias, prolonged fictive silence after TA-sustained fictive overlapping dysrhythmia) as the network reconfigures back to a state of being able to produce a diverse range of fictive patterns (i.e., the critical state). By no means the only explanation for the post-application effects of the neuromodulatory manipulations, it is nonetheless one unexplored framework this present study proposes to understand how neural networks can produce a diversity of output that is both adaptable and innately spontaneous.

Conflicts of Interest

No declared conflict of interest.

Data Availability

The research data supporting this publication can be accessed at https://doi.org/10.17630/84df17ac-77d3-4a61-9bf0-fa6e78a802e1.

Author's Contribution

S.R.P. and W.V.S. conceived the study. W.V.S conducted all experiments, analysis, and visualisation. W.V.S. and S.R.P finalised the figures. S.R.P. supervised the project.

Acknowledgements

This project was made possible by an Industrial CASE PhD studentship (UKRI Biotechnology and Biological Sciences Research Council (BBSRC) grant number BB/T00875X/1) to WVS. This work was additionally supported in part by two Collaborative Research Grants awarded jointly by the Global Office of the University of St Andrews and The Halle Institute for Global Research at Emory University (SRP and A. Prinz), and The Global Office of the University of St Andrews and the University of Bonn (SRP and M. Pankratz), and by a Neurophotonics pump-priming Grant from the RS Macdonald Foundation (SRP and M. Gather).

Supplementary Figures

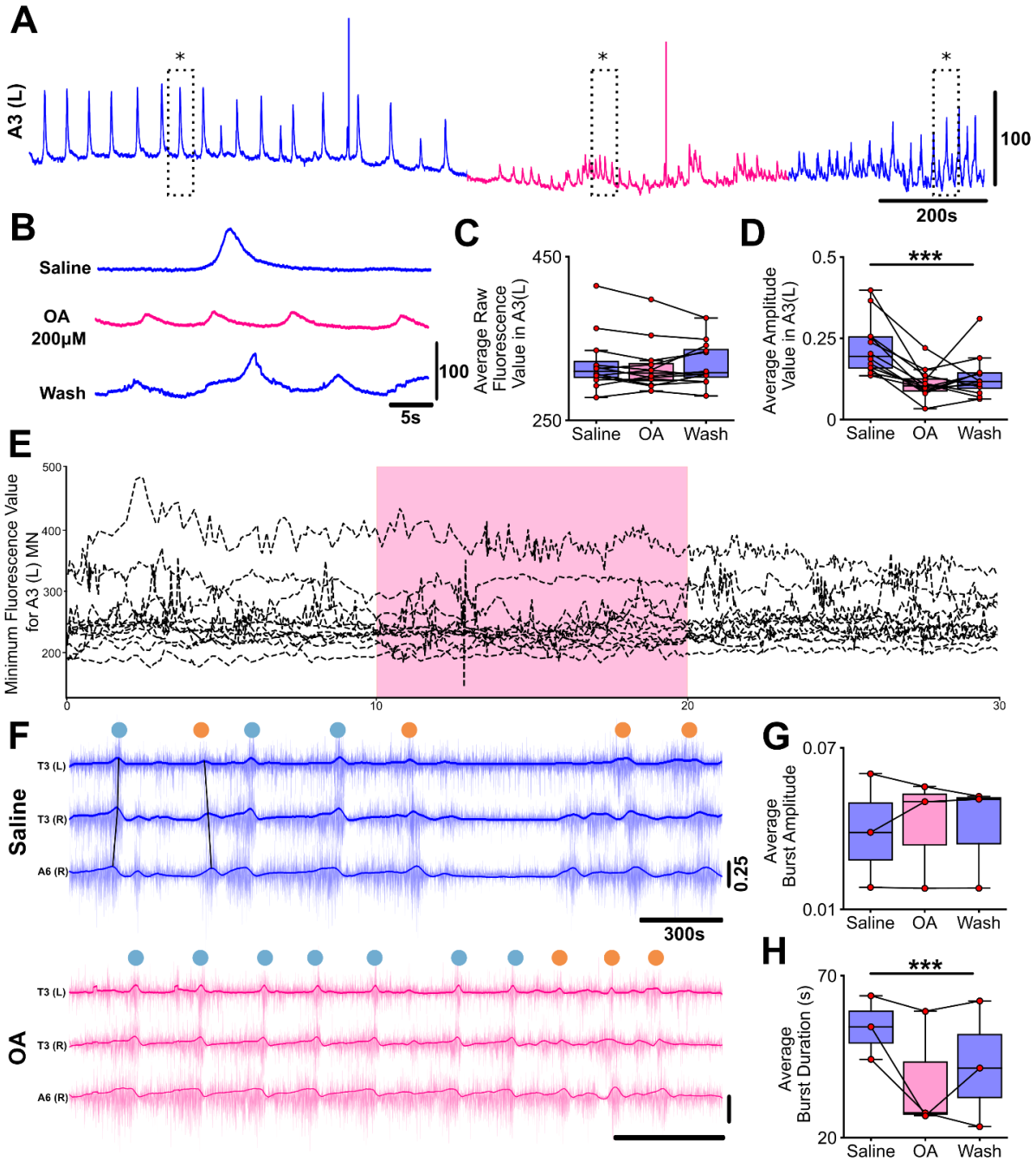

Supplementary Figure 1: Octopamine Decreases Calcium Signal Amplitude and Motor Root Burst Duration Despite No Baseline Change

(**A**) Representative calcium signal trace from A3 left motor neuron before (blue), during 200μM octopamine application (magenta), and after (blue). (**B**) Exemplar activity in the left A3 calcium signal before, during 200μM octopamine application and after. Traces in B are subsections of the total trace denoted by *. (**C**) The average fluorescence value from calcium signal trace before, during, and after 200μM octopamine application. (**D**) The averaged peak amplitude from all A3 motor neuron calcium activity from calcium signal trace before, during, and after 200μM octopamine application across full ventral nerve cord (VNC) perfusion experiments (N=12). (**E**) All traces from full VNC perfusion experiments (grey, dashed line) before, during (magenta box), and after 200μM octopamine application. Note the absence of a visual change in baseline during octopamine application (magenta

box). (**F**) Nerve root recordings for full VNC before (blue) and during (magenta) 200µM octopamine bath application. Yellow lines indicate fictive patterns. Note the elevated frequency of fictive forward wave activity during octopamine application (yellow lines, magenta traces). (**G**) The average amplitude of peaks in A6 motor neurons before and after 200µM octopamine application (N=3). (**H**) The average burst duration of peaks in A7 motor neurons before and after 200µM octopamine application (N=3). Note, the decreased burst duration in motor activity represents calcium activity as a lower signal amplitude. Post-hoc comparison were conducted with p-values: < .5 (*), < .01 (**), <.001 (***) shown. Only statistically significant bars are shown.

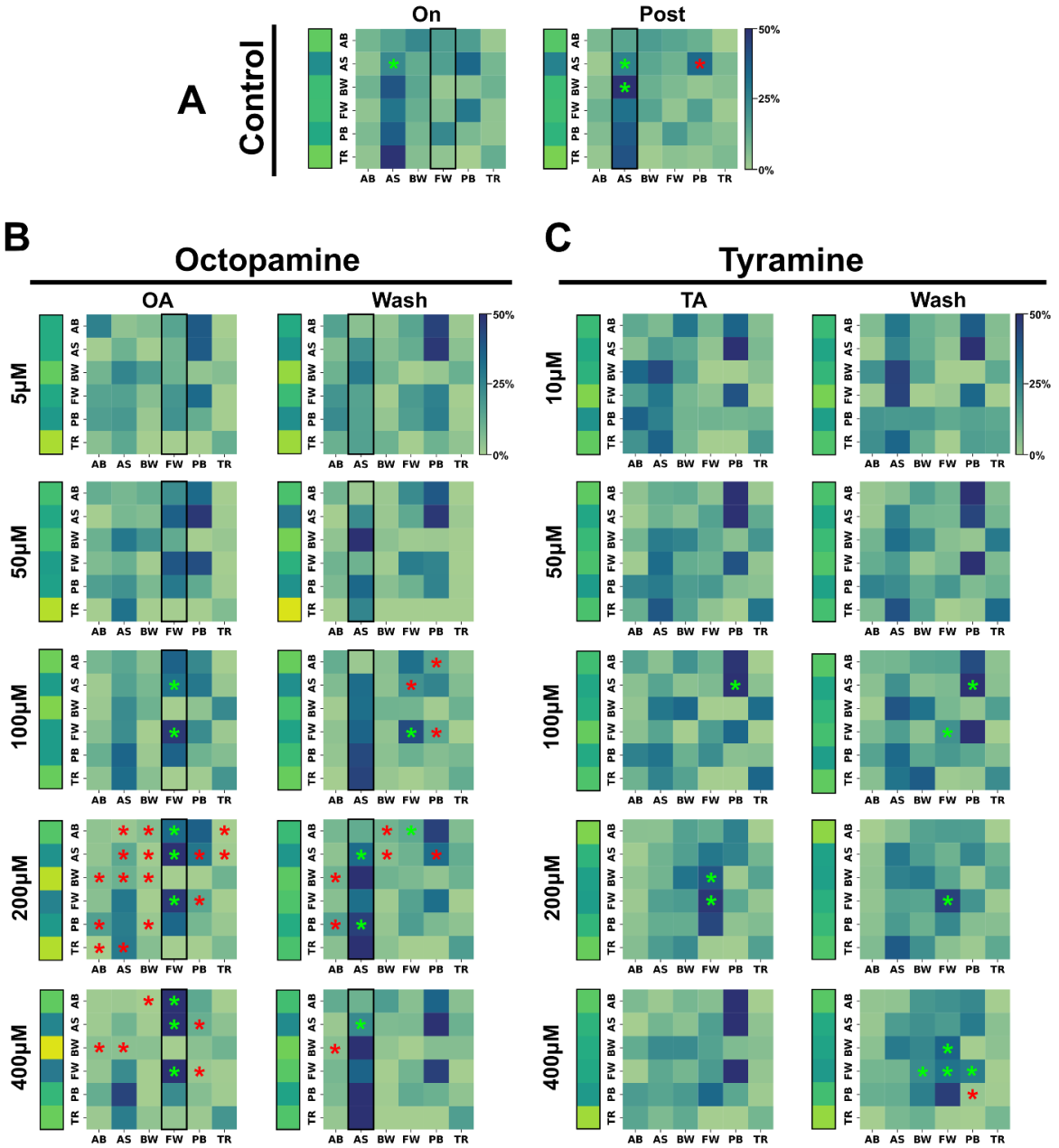

Supplementary Figure 2: Octopamine and Tyramine Alters Motor Competition by Modulation Fictive Transition Probabilities

(**A**) The probability of any fictive behavioural transition (column) to a subsequent fictive program (row) within OK371>GCaMP6m control data (N=28) within the 10 to 20 minute time period ("On") representative of the time period of the neuromodulator perfusion period and > 20 minute time period ("Post) representative of the time period of the neuromodulator wash period. "On" statistical comparisons made between the average transition probabilities

in the 10-20 minute period across all control isolated 3rd instar ventral nerve cords compared to the average transition probabilities in the 0-10 minute period. “Post” statistical comparisons are made between the average transition probabilities in the 20-30 minute period across all control data compared to the average transition probabilities in the 0-10 minute period. (**B**) The average fictive transition probabilities across all the octopamine (OA) concentrations within the application (“On”) and post-application (“Wash”) period. (**C**) The average fictive transition probabilities across all the tyramine (TA) concentrations within the application (“On”) and post-application (“Wash”) period. Post-hoc comparison were conducted with p-values: < .5 (*), < .01 (**), <.001 (***) shown. Only statistically significant bars are shown.

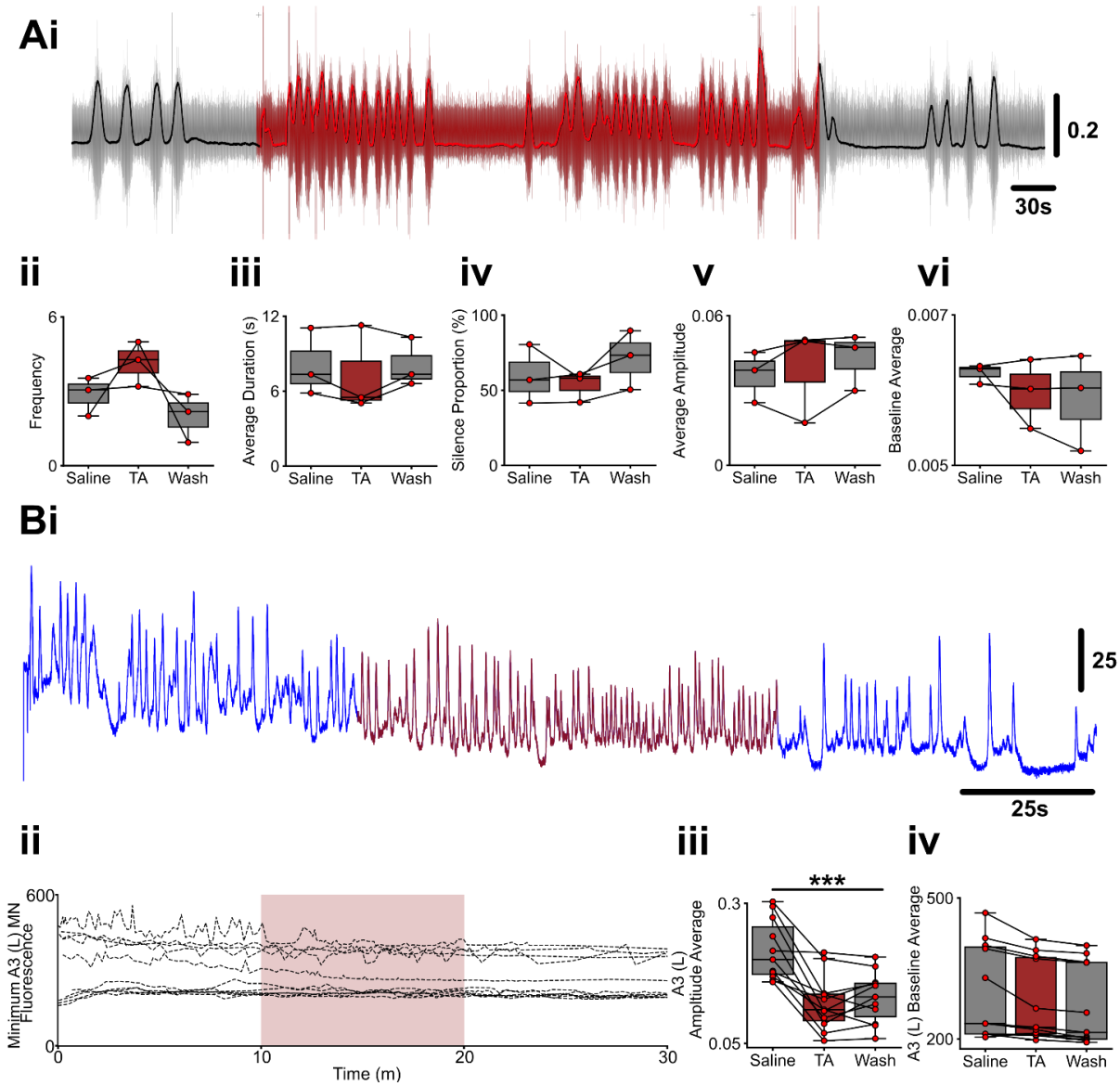

Supplementary Figure 3: Tyramine Shows No Inhibition of Motor Root Activity nor Calcium Baseline

(**A**) Effects of 50μM tyramine bath application on posterior abdominal motor nerve root activity demonstrating (**Ai**) subtle changes to firing patterns (N=3). The effect of 50μM tyramine bath application on posterior abdominal motor root (**Aii**) bursting frequency, (**Aiii**) average burst duration, (**Aiv**), proportion of time (%) without activity > 5% change from baseline, (**Av**) average burst amplitude, and (**Avi**) baseline average for the pre-application (“Saline”), application (“TA”), and post-application (“Wash”) periods. (**B**) Representative effects of 200μM tyramine bath application (dark red) (N=11) on the (**Bi**) calcium activity on the motor neuron pool (abdominal segment 3, left: A3 (L)). (**Bii**) The baseline calcium fluorescence for all isolated ventral nerve cord preparations under 200μM tyramine

bath application (dark red). The effect of 200μM tyramine bath application on (**Biii**) average calcium amplitude across fictive programs and (**Biv**) baseline calcium signal. Post-hoc comparison were conducted with p-values: < .5 (*), < .01 (**), <.001 (***) shown. Only statistically significant bars are shown.

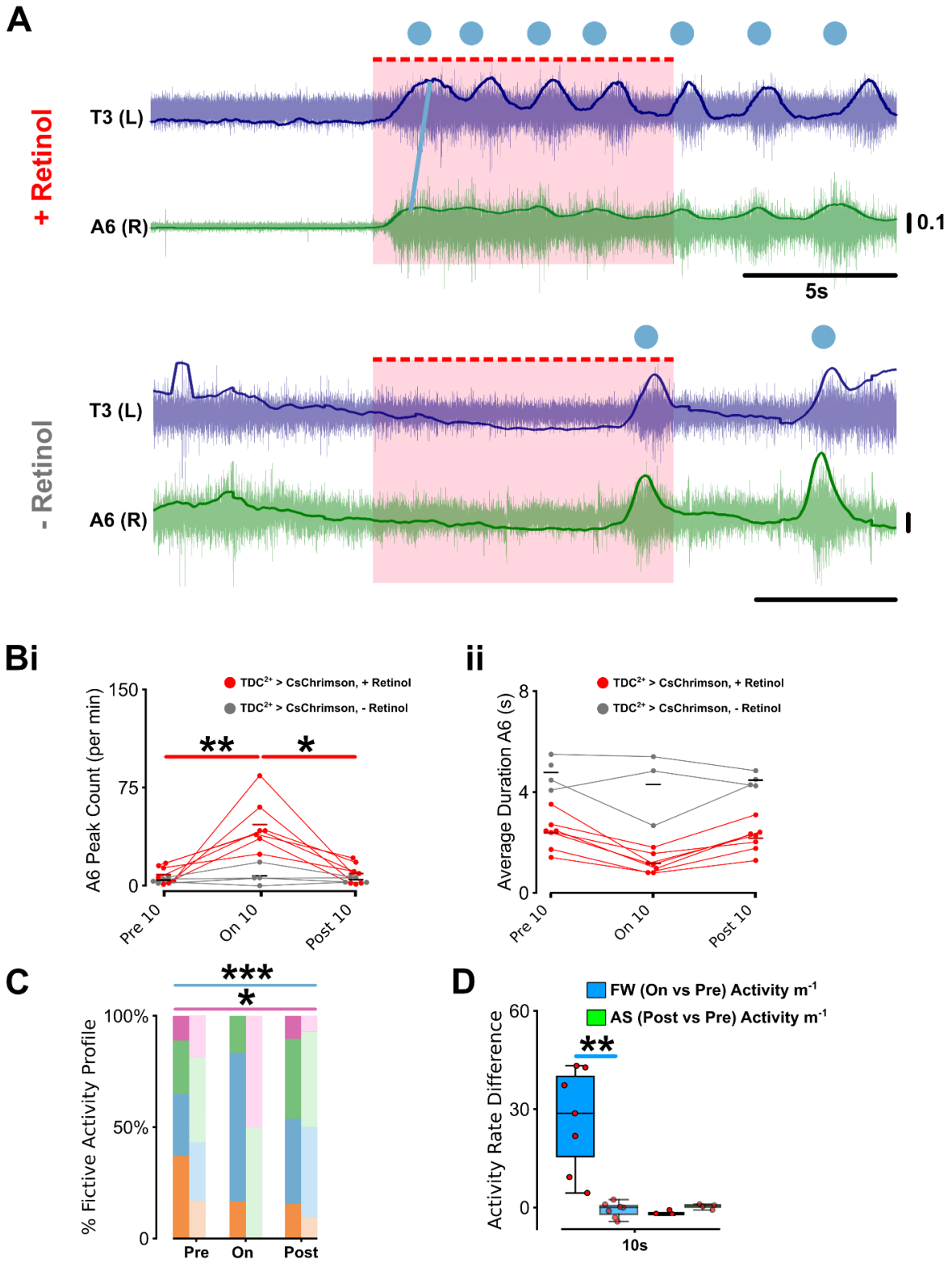

Supplementary Figure 4: Pulsed Stimulation of *tdc*$^{2+}$ Neurons Induces Fictive Forward Bias

(**A**) Representative T3(L) and A6(R) motor root electrophysiology trace demonstrating promotion of fictive forward activity during pulsed stimulation of CsChrimson>*tdc*$^{2+}$ (0.01s, 40Hz, 400 repeats = 10s total stimulation) for experimental (+ retinol) compared to control (- retinol) 3rd instar *Drosophila* larva. (**B**) Quantification of motor root bursting at A6 demonstrating (**i**) peak rate and (**ii**) burst duration changes upon pulsed stimulation (On10) relative to before (Pre10) and after (Post10) stimulation period. (**C**) Quantification of fictive bias before, during, and after pulsed stimulation in preparations where fictive activity could be accurately inferred (N=6). (**D**) The relative fictive activity difference for fictive forward activity during (on) vs before (pre) stimulation (blue) and for anterior asymmetric fictive activity after (post) vs before (pre) stimulation (green). Comparisons followed by post-hoc was conducted with p-values: < .5 (*), < .01 (**), <.001 (***) shown. Only statistically significant bars are shown.

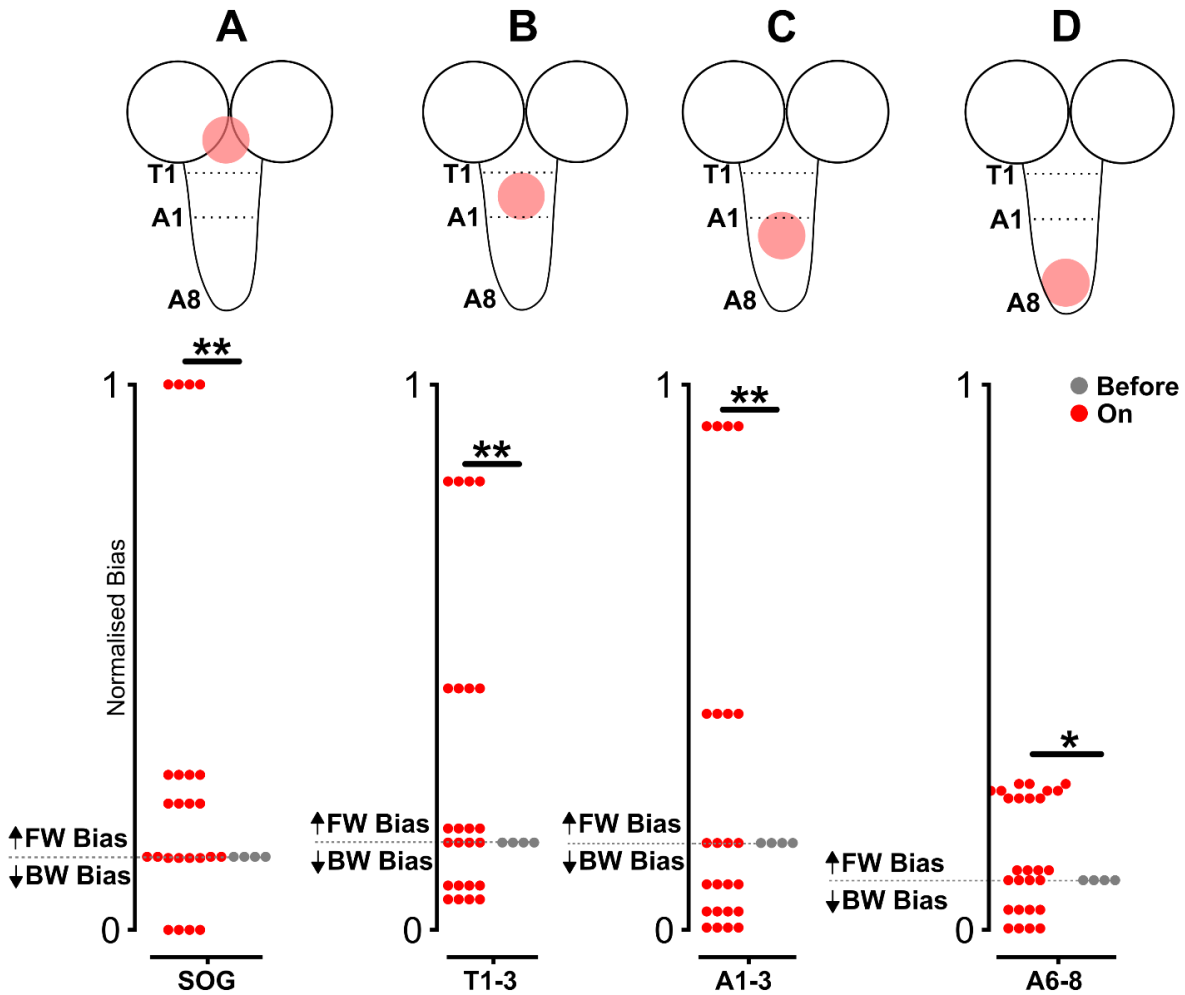

Supplementary Figure 5: Relative Fictive Wave Bias Induced by Restricted Stimulation of *tdc*$^{2+}$ Neurons

Restricted *tdc*$^{2+}$ depolarisation in the (A) SOG, (B), thoracic ganglion (T1-3), (C) anterior abdominal ganglion (A1-3), and (D) posterior abdominal ganglion (A6-8) induces different fictive wave bias in different stimulation periods (N > 2) across all preparations (N = 7). Plots show normalised bias of fictive forward activity rate (m^{-1}) / fictive backward activity rate (m^{-1}) with gray dashed line indicative of relative fictive wave bias before restricted stimulation. Note, across all stimulation periods there are a diverse array of bias changes (i.e., below the level of normalised bias before stimulation = more fictive backward wave bias, above the level of normalised bias before stimulation =

more fictive forward wave bias). Comparisons followed by post-hoc was conducted with p-values: < .5 (*), < .01 (**), <.001 (***) shown. Only statistically significant bars are shown.

References

[1] J. Francis *et al.*, ‘Inhibitory circuit motifs in Drosophila larvae generate motor program diversity and variability’, *PLOS Biol.*, vol. 23, no. 4, p. e3003094, Apr. 2025, doi: 10.1371/journal.pbio.3003094.

[2] T. Jovanic *et al.*, ‘Competitive Disinhibition Mediates Behavioral Choice and Sequences in Drosophila.’, *Cell*, vol. 167, no. 3, pp. 858-870.e19, Oct. 2016, doi: 10.1016/j.cell.2016.09.009.

[3] T. Roeder, ‘The control of metabolic traits by octopamine and tyramine in invertebrates’, *J. Exp. Biol.*, vol. 223, no. 7, p. jeb194282, Apr. 2020, doi: 10.1242/jeb.194282.

[4] T. Farooqui, ‘Review of octopamine in insect nervous systems’, *Open Access Insect Physiol.*, p. 1, June 2012, doi: 10.2147/OAIP.S20911.

[5] Y. Pei, A. Asif-Malik, and J. J. Canales, ‘Trace Amines and the Trace Amine-Associated Receptor 1: Pharmacology, Neurochemistry, and Clinical Implications’, *Front. Neurosci.*, vol. 10, Apr. 2016, doi: 10.3389/fnins.2016.00148.

[6] M. Kutsukake, A. Komatsu, D. Yamamoto, and S. Ishiwa-Chigusa, ‘A tyramine receptor gene mutation causes a defective olfactory behavior in Drosophila melanogaster’, *Gene*, vol. 245, no. 1, pp. 31–42, Mar. 2000, doi: 10.1016/S0378-1119(99)00569-7.

[7] M. Monastirioti, M. Gorczyca, J. Rapus, M. Eckert, K. White, and V. Budnik, ‘Octopamine immunoreactivity in the fruit fly *Drosophila melanogaster*’, *J. Comp. Neurol.*, vol. 356, no. 2, pp. 275–287, May 1995, doi: 10.1002/cne.903560210.

[8] Y. Nagaya, M. Kutsukake, S. I. Chigusa, and A. Komatsu, ‘A trace amine, tyramine, functions as a neuromodulator in Drosophila melanogaster’, *Neurosci. Lett.*, vol. 329, no. 3, pp. 324–328, Sept. 2002, doi: 10.1016/S0304-3940(02)00596-7.

[9] M. Selcho, D. Pauls, B. El Jundi, R. F. Stocker, and A. S. Thum, ‘The Role of octopamine and tyramine in *Drosophila* larval locomotion’, *J. Comp. Neurol.*, vol. 520, no. 16, pp. 3764–3785, Nov. 2012, doi: 10.1002/cne.23152.

[10] M. Vömel and C. Wegener, ‘Neuroarchitecture of Aminergic Systems in the Larval Ventral Ganglion of Drosophila melanogaster’, *PLoS ONE*, vol. 3, no. 3, p. e1848, Mar. 2008, doi: 10.1371/journal.pone.0001848.

[11] T. Farooqui, ‘Octopamine-Mediated Neuromodulation of Insect Senses’, *Neurochem. Res.*, vol. 32, no. 9, pp. 1511–1529, July 2007, doi: 10.1007/s11064-007-9344-7.

[12] M. Selcho, ‘Octopamine in the mushroom body circuitry for learning and memory’, *Learn. Mem.*, vol. 31, no. 5, p. a053839, May 2024, doi: 10.1101/lm.053839.123.

[13] S. C. Hoyer *et al.*, ‘Octopamine in Male Aggression of Drosophila’, *Curr. Biol.*, vol. 18, no. 3, pp. 159–167, Feb. 2008, doi: 10.1016/j.cub.2007.12.052.

[14] I. K. Yakovlev, ‘Effects of Octopamine on Aggressive Behavior in Red Wood Ants’, *Neurosci. Behav. Physiol.*, vol. 48, no. 3, pp. 279–288, Mar. 2018, doi: 10.1007/s11055-018-0561-0.

[15] P. A. Stevenson, V. Dyakonova, J. Rillich, and K. Schildberger, ‘Octopamine and Experience-Dependent Modulation of Aggression in Crickets’, *J. Neurosci.*, vol. 25, no. 6, pp. 1431–1441, Feb. 2005, doi: 10.1523/JNEUROSCI.4258-04.2005.

[16] K. Mizutani, H. Ogawa, J. Saito, and K. Oka, ‘Fictive locomotion induced by octopamine in the earthworm’, *J. Exp. Biol.*, vol. 205, no. 2, pp. 265–271, Jan. 2002, doi: 10.1242/jeb.205.2.265.

[17] I. Orchard, J. M. Ramirez, and A. B. Lange, ‘A Multifunctional Role for Octopamine in Locust Flight’, *Annu. Rev. Entomol.*, vol. 38, no. 1, pp. 227–249, Jan. 1993, doi: 10.1146/annurev.en.38.010193.001303.

[18] J. C. Ormshaw and C. J. H. Elliott, ‘Octopamine boosts snail locomotion: behavioural and cellular analysis’, *Invert. Neurosci.*, vol. 6, no. 4, pp. 215–220, Nov. 2006, doi: 10.1007/s10158-006-0031-1.

[19] T. Roeder, ‘TYRAMINE AND OCTOPAMINE: Ruling Behavior and Metabolism’, *Annu. Rev. Entomol.*, vol. 50, no. 1, pp. 447–477, Jan. 2005, doi: 10.1146/annurev.ento.50.071803.130404.

[20] D. J. Candy, ‘The regulation of locust flight muscle metabolism by octopamine and other compounds’, *Insect Biochem.*, vol. 8, no. 3, pp. 177–181, Jan. 1978, doi: 10.1016/0020-1790(78)90070-7.

[21] Y. Li *et al.*, ‘Octopamine controls starvation resistance, life span and metabolic traits in Drosophila’, *Sci. Rep.*, vol. 6, no. 1, p. 35359, Oct. 2016, doi: 10.1038/srep35359.

[22] A. C. Koon and V. Budnik, ‘Inhibitory Control of Synaptic and Behavioral Plasticity by Octopaminergic Signaling’, *J. Neurosci.*, vol. 32, no. 18, pp. 6312–6322, May 2012, doi: 10.1523/JNEUROSCI.6517-11.2012.

[23] A. C. Koon *et al.*, ‘Autoregulatory and paracrine control of synaptic and behavioral plasticity by octopaminergic signaling’, *Nat. Neurosci.*, vol. 14, no. 2, pp. 190–199, Feb. 2011, doi: 10.1038/nn.2716.

[24] Z. Yang, Y. Yu, V. Zhang, Y. Tian, W. Qi, and L. Wang, ‘Octopamine mediates starvation-induced hyperactivity in adult *Drosophila*’, *Proc. Natl. Acad. Sci.*, vol. 112, no. 16, pp. 5219–5224, Apr. 2015, doi: 10.1073/pnas.1417838112.

[25] A. Sujkowski, D. Ramesh, A. Brockmann, and R. Wessells, ‘Octopamine Drives Endurance Exercise Adaptations in Drosophila’, *Cell Rep.*, vol. 21, no. 7, pp. 1809–1823, Nov. 2017, doi: 10.1016/j.celrep.2017.10.065.

[26] B. Brembs, F. Christiansen, H. J. Pflüger, and C. Duch, ‘Flight Initiation and Maintenance Deficits in Flies with Genetically Altered Biogenic Amine Levels’, *J. Neurosci.*, vol. 27, no. 41, pp. 11122–11131, Oct. 2007, doi: 10.1523/JNEUROSCI.2704-07.2007.

[27] S. Saraswati, L. E. Fox, D. R. Soll, and C. Wu, ‘Tyramine and octopamine have opposite effects on the locomotion of *Drosophila* larvae’, *J. Neurobiol.*, vol. 58, no. 4, pp. 425–441, Mar. 2004, doi: 10.1002/neu.10298.

[28] L. E. Fox, D. R. Soll, and C.-F. Wu, ‘Coordination and Modulation of Locomotion Pattern Generators in *Drosophila* Larvae: Effects of Altered Biogenic Amine Levels by the Tyramine β Hydroxlyase Mutation’, *J. Neurosci.*, vol. 26, no. 5, pp. 1486–1498, Feb. 2006, doi: 10.1523/JNEUROSCI.4749-05.2006.

[29] H. Hashemzadeh-Gargari and W. Otto Friesen, ‘Modulation of swimming activity in the medicinal leech by serotonin and octopamine’, *Comp. Biochem. Physiol. Part C Comp. Pharmacol.*, vol. 94, no. 1, pp. 295–302, Jan. 1989, doi: 10.1016/0742-8413(89)90182-5.

[30] B. Johnson and R. Harris-Warrick, ‘Aminergic modulation of graded synaptic transmission in the lobster stomatogastric ganglion’, *J. Neurosci.*, vol. 10, no. 7, pp. 2066–2076, July 1990, doi: 10.1523/JNEUROSCI.10-07-02066.1990.

[31] S. C. Kinnamon, L. W. Klaassen, A. E. Kammer, and D. Claassen, ‘Octopamine and chlordimeform enhance sensory responsiveness and production of the flight motor pattern in developing and adult moths’, *J. Neurobiol.*, vol. 15, no. 4, pp. 283–293, July 1984, doi: 10.1002/neu.480150405.

[32] J. M. Ramirez and K. G. Pearson, ‘Octopaminergic modulation of interneurons in the flight system of the locust’, *J. Neurophysiol.*, vol. 66, no. 5, pp. 1522–1537, Nov. 1991, doi: 10.1152/jn.1991.66.5.1522.

[33] M. J. Alkema, M. Hunter-Ensor, N. Ringstad, and H. R. Horvitz, ‘Tyramine Functions Independently of Octopamine in the Caenorhabditis elegans Nervous System’, *Neuron*, vol. 46, no. 2, pp. 247–260, Apr. 2005, doi: 10.1016/j.neuron.2005.02.024.

[34] N. Schützler *et al.*, ‘Tyramine action on motoneuron excitability and adaptable tyramine/octopamine ratios adjust *Drosophila* locomotion to nutritional state’, *Proc. Natl. Acad. Sci.*, vol. 116, no. 9, pp. 3805–3810, Feb. 2019, doi: 10.1073/pnas.1813554116.

[35] B. Mulloney, L. D. Acevedo, and A. G. Bradbury, ‘Modulation of the crayfish swimmeret rhythm by octopamine and the neuropeptide proctolin’, *J. Neurophysiol.*, vol. 58, no. 3, pp. 584–597, Sept. 1987, doi: 10.1152/jn.1987.58.3.584.
[36] A. D. McClellan, G. D. Brown, and P. A. Getting, ‘Modulation of swimming in Tritonia: excitatory and inhibitory effects of serotonin’, *J. Comp. Physiol. A*, vol. 174, no. 2, Feb. 1994, doi: 10.1007/BF00193792.
[37] K. Nishikawa and Y. Kidokoro, ‘Octopamine inhibits synaptic transmission at the larval neuromuscular junction in Drosophila melanogaster’, *Brain Res.*, vol. 837, no. 1–2, pp. 67–74, Aug. 1999, doi: 10.1016/S0006-8993(99)01676-5.
[38] Z.-T. Zhu, A. C. Munhall, and S. W. Johnson, ‘Tyramine excites rat subthalamic neurons in vitro by a dopamine-dependent mechanism’, *Neuropharmacology*, vol. 52, no. 4, pp. 1169–1178, Mar. 2007, doi: 10.1016/j.neuropharm.2006.12.005.
[39] A. Donini and A. B. Lange, ‘Evidence for a possible neurotransmitter/neuromodulator role of tyramine on the locust oviducts’, *J. Insect Physiol.*, vol. 50, no. 4, pp. 351–361, Apr. 2004, doi: 10.1016/j.jinsphys.2004.02.005.
[40] C. McClung and J. Hirsh, ‘The trace amine tyramine is essential for sensitization to cocaine in Drosophila’, *Curr. Biol.*, vol. 9, no. 16, pp. 853–860, Aug. 1999, doi: 10.1016/S0960-9822(99)80389-3.
[41] M. A. El-Brolosy and D. Y. R. Stainier, ‘Genetic compensation: A phenomenon in search of mechanisms’, *PLOS Genet.*, vol. 13, no. 7, p. e1006780, July 2017, doi: 10.1371/journal.pgen.1006780.
[42] A. A. Prinz, D. Bucher, and E. Marder, ‘Similar network activity from disparate circuit parameters’, *Nat. Neurosci.*, vol. 7, no. 12, pp. 1345–1352, Dec. 2004, doi: 10.1038/nn1352.
[43] E. Marder, ‘Neuromodulation of Neuronal Circuits: Back to the Future’, *Neuron*, vol. 76, no. 1, pp. 1–11, Oct. 2012, doi: 10.1016/j.neuron.2012.09.010.
[44] E. Marder, ‘Variability, compensation, and modulation in neurons and circuits’, *Proc. Natl. Acad. Sci.*, vol. 108, no. supplement_3, pp. 15542–15548, Sept. 2011, doi: 10.1073/pnas.1010674108.
[45] S. H. Cole, G. E. Carney, C. A. McClung, S. S. Willard, B. J. Taylor, and J. Hirsh, ‘Two Functional but Noncomplementing Drosophila Tyrosine Decarboxylase Genes’, *J. Biol. Chem.*, vol. 280, no. 15, pp. 14948–14955, Apr. 2005, doi: 10.1074/jbc.M414197200.
[46] M. Monastirioti, C. E. Linn, Jr., and K. White, ‘Characterization of ***Drosophila Tyramine β-Hydroxylase*** Gene and Isolation of Mutant Flies Lacking Octopamine’, *J. Neurosci.*, vol. 16, no. 12, pp. 3900–3911, June 1996, doi: 10.1523/JNEUROSCI.16-12-03900.1996.
[47] S. Busch, M. Selcho, K. Ito, and H. Tanimoto, ‘A map of octopaminergic neurons in the *Drosophila* brain’, *J. Comp. Neurol.*, vol. 513, no. 6, pp. 643–667, Apr. 2009, doi: 10.1002/cne.21966.
[48] M. Selcho, D. Pauls, A. Huser, R. F. Stocker, and A. S. Thum, ‘Characterization of the octopaminergic and tyraminergic neurons in the central brain of *Drosophila* larvae’, *J. Comp. Neurol.*, vol. 522, no. 15, pp. 3485–3500, Oct. 2014, doi: 10.1002/cne.23616.
[49] S. R. Pulver, T. G. Bayley, A. L. Taylor, J. Berni, M. Bate, and B. Hedwig, ‘Imaging fictive locomotor patterns in larval Drosophila.’, *J. Neurophysiol.*, vol. 114, no. 5, pp. 2564–2577, Nov. 2015, doi: 10.1152/jn.00731.2015.
[50] W. C. Lemon *et al.*, ‘Whole-central nervous system functional imaging in larval Drosophila.’, *Nat. Commun.*, vol. 6, p. 7924, Aug. 2015, doi: 10.1038/ncomms8924.
[51] A. Sordillo and C. I. Bargmann, ‘Behavioral control by depolarized and hyperpolarized states of an integrating neuron’, *eLife*, vol. 10, p. e67723, Nov. 2021, doi: 10.7554/eLife.67723.
[52] J. K. Pirri, A. D. McPherson, J. L. Donnelly, M. M. Francis, and M. J. Alkema, ‘A Tyramine-Gated Chloride Channel Coordinates Distinct Motor Programs of a Caenorhabditis elegans Escape Response’, *Neuron*, vol. 62, no. 4, pp. 526–538, May 2009, doi: 10.1016/j.neuron.2009.04.013.

[53] Y. Kagawa-Nagamura, K. Gengyo-Ando, M. Ohkura, and J. Nakai, ‘Role of tyramine in calcium dynamics of GABAergic neurons and escape behavior in Caenorhabditis elegans’, *Zool. Lett.*, vol. 4, no. 1, p. 19, Dec. 2018, doi: 10.1186/s40851-018-0103-1.
[54] J. Meng *et al.*, ‘A tonically active master neuron modulates mutually exclusive motor states at two timescales’, *Sci. Adv.*, vol. 10, no. 15, p. eadk0002, Apr. 2024, doi: 10.1126/sciadv.adk0002.
[55] J. Y. H. Wong *et al.*, ‘Octopaminergic neurons have multiple targets in *Drosophila* larval mushroom body calyx and can modulate behavioral odor discrimination’, *Learn. Mem.*, vol. 28, no. 2, pp. 53–71, Feb. 2021, doi: 10.1101/lm.052159.120.
[56] R. Marley and R. A. Baines, ‘Dissection of Third-Instar *Drosophila* Larvae for Electrophysiological Recording from Neurons’, *Cold Spring Harb. Protoc.*, vol. 2011, no. 9, p. pdb.prot065656, Sept. 2011, doi: 10.1101/pdb.prot065656.
[57] A. Edelstein, N. Amodaj, K. Hoover, R. Vale, and N. Stuurman, ‘Computer Control of Microscopes Using µManager’, *Curr. Protoc. Mol. Biol.*, vol. 92, no. 1, Oct. 2010, doi: 10.1002/0471142727.mb1420s92.
[58] C. A. Schneider, W. S. Rasband, and K. W. Eliceiri, ‘NIH Image to ImageJ: 25 years of image analysis’, *Nat. Methods*, vol. 9, no. 7, pp. 671–675, July 2012, doi: 10.1038/nmeth.2089.
[59] J. Schindelin *et al.*, ‘Fiji: an open-source platform for biological-image analysis’, *Nat. Methods*, vol. 9, no. 7, pp. 676–682, July 2012, doi: 10.1038/nmeth.2019.
[60] W. J. Heitler, ‘Practical tools for analysing rhythmic neural activity’, *J. Neurosci. Methods*, vol. 185, no. 1, pp. 151–164, Dec. 2009, doi: 10.1016/j.jneumeth.2009.09.009.
[61] J. Berni, ‘Genetic dissection of a regionally differentiated network for exploratory behavior in Drosophila larvae.’, *Curr. Biol. CB*, vol. 25, no. 10, pp. 1319–1326, May 2015, doi: 10.1016/j.cub.2015.03.023.
[62] A. Debnath, P. D. E. Williams, and B. A. Bamber, ‘Reduced Ca2+ transient amplitudes may signify increased or decreased depolarization depending on the neuromodulatory signaling pathway’, *Front. Neurosci.*, vol. 16, p. 931328, July 2022, doi: 10.3389/fnins.2022.931328.
[63] S. Ryglewski, C. Duch, and B. Altenhein, ‘Tyramine Actions on Drosophila Flight Behavior Are Affected by a Glial Dehydrogenase/Reductase’, *Front. Syst. Neurosci.*, vol. 11, p. 68, Sept. 2017, doi: 10.3389/fnsys.2017.00068.
[64] M. Winding *et al.*, ‘The connectome of an insect brain’, *Science*, vol. 379, no. 6636, p. eadd9330, Mar. 2023, doi: 10.1126/science.add9330.
[65] T. Stürner *et al.*, ‘Comparative connectomics of the descending and ascending neurons of the *Drosophila* nervous system: stereotypy and sexual dimorphism’, June 06, 2024. doi: 10.1101/2024.06.04.596633.
[66] A. A. Zarin, B. Mark, A. Cardona, A. Litwin-Kumar, and C. Q. Doe, ‘A multilayer circuit architecture for the generation of distinct locomotor behaviors in *Drosophila*’, *eLife*, vol. 8, p. e51781, Dec. 2019, doi: 10.7554/eLife.51781.
[67] A. Fushiki, M. F. Zwart, H. Kohsaka, R. D. Fetter, A. Cardona, and A. Nose, ‘A circuit mechanism for the propagation of waves of muscle contraction in Drosophila’, *eLife*, vol. 5, p. e13253, Feb. 2016, doi: 10.7554/eLife.13253.
[68] A. Carreira-Rosario *et al.*, ‘MDN brain descending neurons coordinately activate backward and inhibit forward locomotion’, *eLife*, vol. 7, p. e38554, Aug. 2018, doi: 10.7554/eLife.38554.
[69] A. Zhao *et al.*, ‘High-ambition climate action in all sectors can achieve a 65% greenhouse gas emissions reduction in the United States by 2035’, *Npj Clim. Action*, vol. 3, no. 1, p. 63, July 2024, doi: 10.1038/s44168-024-00145-x.
[70] U. Černe *et al.*, ‘Ca^{2+} excitability of glia to neuromodulator octopamine in *Drosophila* living brain is greater than that of neurons’, *Acta Physiol.*, vol. 241, no. 2, p. e14270, Feb. 2025, doi: 10.1111/apha.14270.

[71] S. El-Kholy, F. Stephano, Y. Li, A. Bhandari, C. Fink, and T. Roeder, ‘Expression analysis of octopamine and tyramine receptors in Drosophila’, *Cell Tissue Res.*, vol. 361, no. 3, pp. 669–684, Sept. 2015, doi: 10.1007/s00441-015-2137-4.

[72] L. M. Sherer *et al.*, ‘Octopamine neuron dependent aggression requires dVGLUT from dual-transmitting neurons’, *PLOS Genet.*, vol. 16, no. 2, p. e1008609, Feb. 2020, doi: 10.1371/journal.pgen.1008609.

[73] C.-L. Wu, M.-F. M. Shih, P.-T. Lee, and A.-S. Chiang, ‘An Octopamine-Mushroom Body Circuit Modulates the Formation of Anesthesia-Resistant Memory in Drosophila’, *Curr. Biol.*, vol. 23, no. 23, pp. 2346–2354, Dec. 2013, doi: 10.1016/j.cub.2013.09.056.

[74] J. Li and W. L. Shew, ‘Tuning network dynamics from criticality to an asynchronous state’, *PLOS Comput. Biol.*, vol. 16, no. 9, p. e1008268, Sept. 2020, doi: 10.1371/journal.pcbi.1008268.

[75] B. Ermentrout, ‘Complex dynamics in winner-take-all neural nets with slow inhibition’, *Neural Netw.*, vol. 5, no. 3, pp. 415–431, Jan. 1992, doi: 10.1016/0893-6080(92)90004-3.

[76] Z.-H. Mao and S. G. Massaquoi, ‘Dynamics of Winner-Take-All Competition in Recurrent Neural Networks With Lateral Inhibition’, *IEEE Trans. Neural Netw.*, vol. 18, no. 1, pp. 55–69, Jan. 2007, doi: 10.1109/TNN.2006.883724.

[77] R. Pang, ‘Balanced state of networks of winner-take-all units’, *PLOS Comput. Biol.*, vol. 21, no. 6, p. e1013081, June 2025, doi: 10.1371/journal.pcbi.1013081.

[78] K. Feng *et al.*, ‘A central steering circuit in *Drosophila*’, July 02, 2024, *Neuroscience*. doi: 10.1101/2024.06.27.601106.

[79] L. Zeng, J. Feng, and W. Lu, ‘A general description of criticality in neural network models’, *Heliyon*, vol. 10, no. 5, p. e27183, Mar. 2024, doi: 10.1016/j.heliyon.2024.e27183.

[80] J. O’Byrne and K. Jerbi, ‘How critical is brain criticality?’, *Trends Neurosci.*, vol. 45, no. 11, pp. 820–837, Nov. 2022, doi: 10.1016/j.tins.2022.08.007.